



## **Master Thesis**

**Antifouling polymeric membranes prepared by non-solvent induced phase separation (NIPS) technique for separation of contaminated wastewater**

*Study programme:* N0723A270002 Textile Engineering

*Author:* **Bharti Bisen, B.A.**

*Thesis Supervisors:* doc. Fatma Yalcinkaya, MSc. Ph.D.  
Institute of Mechatronics and Computer  
Engineering

Liberec 2024



## Master Thesis Assignment Form

Antifouling polymeric membranes prepared by non-solvent induced phase separation (NIPS) technique for separation of contaminated wastewater

*Name and surname:* **Bharti Bisen, B.A.**  
*Identification number:* T21000321  
*Study programme:* N0723A270002 Textile Engineering  
*Assigning department:* Department of Nonwovens and Nanofibrous materials  
*Academic year:* 2022/2023

### Rules for Elaboration:

1. Literature research on microplastics removals by using membrane technology.
2. Understanding the non-solvent induced phase separation (NIPS) for the synthesis of membranes.
3. Understanding surface modification of NIPS membrane using micro- and nano-particles.
4. Experimental set-up and design.
5. Characterize the synthesized membranes and test their microplastic rejection and water permeability.
6. Evaluate the results and discuss the findings.
7. Conclude the work with main findings and propose further measures.

*Scope of Graphic Work:* as required  
*Scope of Report:* 40-60  
*Thesis Form:* printed/electronic  
*Thesis Language:* English

#### List of Specialised Literature:

1. Thesis of Thi Diem Trang Nguyen, Preparation and Characterization of Membranes Formed by Non-Solvent Induced Phase Separation (NIPS), Faculty of Textile, TUL, Liberec, 2022.
2. Valizadeh, K., Heydarinasab, A., Hosseini, S.S. and Bazgir, S., 2021. Preparation of modified membrane of polyvinylidene fluoride (PVDF) and evaluation of anti-fouling features and high capability in water/oil emulsion separation. Journal of the Taiwan Institute of Chemical Engineers, 126, pp.36-49.
3. Wang, Q., Cui, J., Xie, A., Lang, J., Li, C. and Yan, Y., 2020. PVDF composite membrane with robust UV-induced self-cleaning performance for durable oil/water emulsions separation. Journal of the Taiwan Institute of Chemical Engineers, 110, pp.130-139.
4. Garcia JU. Understanding Membrane Formation in Nonsolvent-Induced Phase Separation. University of California, Santa Barbara; 2020.
5. Coveney S. Fundamentals of Phase Separation in Polymer Blend Thin Films. Springer; 2015 Jun 18.

*Thesis Supervisors:* doc. Fatma Yalcinkaya, MSc. Ph.D.  
Institute of Mechatronics and Computer  
Engineering

*Date of Thesis Assignment:* November 1, 2022

*Date of Thesis Submission:* May 20, 2024

L.S.

doc. Ing. Vladimír Bajzík, Ph.D.  
Dean

prof. Ing. Jakub Wiener, Ph.D.  
Study programme guarantor

Liberec November 1, 2022

# Declaration

I hereby certify, I, myself, have written my master thesis as an original and primary work using the literature listed below and consulting it with my thesis supervisor and my thesis counsellor.

I acknowledge that my master thesis is fully governed by Act No. 121/2000 Coll., the Copyright Act, in particular Article 60 -School Work.

I acknowledge that the Technical University of Liberec does not infringe on my copyrights by using my master thesis for internal purposes of the Technical University of Liberec.

I am aware of my obligation to inform the Technical University of Liberec on having used or granted license to use the results of my master thesis; in such a case the Technical University of Liberec may require reimbursement of the costs incurred for creating the result up to their actual amount.

At the same time, I honestly declare that the text of the printed version of my master thesis is identical with the text of the electronic version uploaded into the IS/STAG.

I acknowledge that the Technical University of Liberec will make my master thesis public in accordance with paragraph 47b of Act No. 111/1998 Coll., on Higher Education Institutions and on Amendment to Other Acts (the Higher Education Act), as amended.

I am aware of the consequences which may under the Higher Education Act result from a breach of this declaration.

May 16, 2024

Bharti Bisen, B.A.

## **ACKNOWLEDGMENT**

It pleases me immensely to recount the people who have helped me through my endeavors, sometimes by just “being a friend or a dedicated ear that listened” and sometimes by helping me technically or philosophically overcome the research hurdles. I want to thank my supervisor, Doc. Fatma Yalcinkaya, MSc. Ph.D., who has been lending her valuable time and knowledge to my research work whenever it was possible. This research work would not have been possible without her assistance. Also, I would like to thank Ing. Hana Musilova For their cooperation and motivation for the diploma thesis.

Liberec

**20.05.24**

Bharti Nirmala-Narayan Bisen.

## Abstract

This thesis investigates the fabrication of polyvinylidene fluoride (PVDF) membranes with enhanced antifouling properties for the separation of contaminated wastewater, particularly focusing on microplastic removal. The membranes were prepared using the non-solvent induced phase separation (NIPS) technique, incorporating micro and nanoparticles to improve their performance. The study examines PVDF membranes with 15% and 20% weight concentrations, analyzing their surface properties, hydrophilicity, stability, and rejection rates through various characterization techniques including SEM-EDS, pore size analysis, FTIR, water contact angle measurement, and swelling tests.

The SEM-EDS analysis confirmed the presence of micro- and nano-particles on the membrane surfaces. SEM images revealed that the membranes exhibited no cracks or visible damage. FTIR results provided evidence of chemical modification to the membranes. Swelling tests indicated a slight increase in membrane swelling after immersion in water, while maintaining dimensional stability. The findings corroborate the presence of micro and nanoparticles on the membrane surface, which alter its properties, enhancing hydrophilicity. Permeability tests showed that the membranes are permeable under low applied pressure. Antifouling performance was evaluated through three successive membrane tests, with minimal water rinsing between each run. Results demonstrated that unmodified membranes experienced significant fouling after the first run, while modification enabled the membrane to function for second and third runs. However, permeability decreased with each successive run.

Although modifications extended the membrane's filtration lifespan, reducing operational costs, fouling remains inevitable. Periodic cleaning procedures will be necessary to maintain membrane performance.

In summary, this thesis underscores the potential of micro and nanoparticles in membrane modification, offering promising solutions for microplastic pollution in water treatment. The experiment, conducted at a laboratory scale, suggests avenues for further research including varying PVDF and nanoparticle concentrations to optimize membrane permeability and antifouling properties and measurement of leaching of micro- and nano-particles to water. These membranes hold promise for implementation in water treatment systems, contributing to the purification of drinking water and protection of aquatic ecosystems from the harmful effects of microplastic contamination.

**Keywords:** PVDF, NIPS, Microplastic Filtration, Antifouling

## Abstrakt

Tato diplomová práce zkoumá výrobu membrán z polyvinylidenfluoridu (PVDF) s vylepšenými protihnilobnými vlastnostmi pro separaci znečištěných odpadních vod, zejména se zaměřením na odstraňování mikroplastů. Membrány byly připraveny pomocí techniky fázové separace bez použití rozpouštědla (NIPS), přičemž pro zlepšení jejich účinnosti byly použity mikročástice a nanočástice. Studie zkoumá membrány PVDF s 15% a 20% hmotnostní koncentrací, analyzuje jejich povrchové vlastnosti, hydrofilitu, stabilitu a míru rejekce pomocí různých charakterizačních technik včetně SEM-EDS, analýzy velikosti pórů, FTIR, měření kontaktního úhlu s vodou a testů bobtnavosti.

Analýza SEM-EDS potvrdila přítomnost mikro a nanočástic na povrchu membrán. SEM snímky ukázaly, že membrány nevykazují žádné trhliny ani viditelné poškození. Výsledky FTIR prokázaly chemickou modifikaci membrán. Testy bobtnavosti naznačily mírný nárůst bobtnání membrán po ponoření do vody, při zachování rozměrové stability. Tato zjištění potvrzují přítomnost mikro a nanočástic na povrchu membrány, které mění její vlastnosti a zvyšují hydrofilitu. Testy propustnosti ukázaly, že membrány jsou propustné i při nízkém tlaku. Účinnost proti zanášení byla hodnocena třemi po sobě jdoucími testy membrán, přičemž mezi jednotlivými zkouškami bylo provedeno minimální oplachování vodou. Výsledky ukázaly, že u nemodifikovaných membrán došlo k výraznému znečištění po prvním běhu, zatímco modifikace umožnila funkčnost membrány při druhém a třetím běhu. Propustnost se však s každým dalším pokusem snižovala.

Přestože úpravy prodloužily životnost membrány a snížily provozní náklady, zanášení zůstává nevyhnutelné. K udržení výkonnosti membrány bude nutné provádět pravidelné čištění.

Závěrem lze říci, že tato práce podtrhuje potenciál mikročástic a nanočástic při modifikaci membrán a nabízí slibná řešení znečištění vody mikroplasty. Experiment, provedený v laboratorním měřítku, naznačuje cesty pro další výzkum, včetně změny koncentrace PVDF a nanočástic za účelem optimalizace propustnosti membrán a vlastností proti zanášení a měření úniku mikročástic a nanočástic do vody. Tyto membrány jsou slibné pro použití v systémech úpravy vody, což přispěje k čištění pitné vody a ochraně vodních ekosystémů před škodlivými účinky kontaminace mikroplasty.

**Klíčová slova:** PVDF, NIPS, mikroplastová filtrace, ochrana proti znečištění

# Contents

<b>1. Introduction</b> .....	12
<b>1.1 Background and Significance</b> .....	12
<b>1.2 Scope and limitation</b> .....	15
<b>2. Literature Review</b> .....	18
<b>2.1 Membrane Technology in Wastewater Treatment</b> .....	18
<b>2.1.1 Asymmetric membrane</b> .....	21
<b>2.1.2 Membrane Process for Microplastic Removal</b> .....	22
<b>2.2 Polymers Used in Membrane Technology</b> .....	25
<b>3. Aim of the thesis</b> .....	28
<b>4 Materials, Equipment &amp; Method</b> .....	29
<b>4.1 Material selection</b> .....	29
<b>4.2 Material and membrane Preparation</b> .....	29
<b>4.3 Surface Modification of Membrane</b> .....	31
<b>4.4 Filtration Test</b> .....	31
<b>4.5 Turbidity Test</b> .....	32
<b>4.6 Permeability and Rejection</b> .....	33
<b>4.7 Membrane Characterization</b> .....	34
<b>4.7.1 Fourier transformed infrared Spectroscopy</b> .....	34
<b>4.7.2 SEM-EDS</b> .....	35
<b>4.7.3 Contact Angle</b> .....	35
<b>4.7.4 Water uptake and swelling of the membrane</b> .....	38
<b>5. Result &amp; Discussion</b> .....	39
<b>5.1 Membrane Characterization</b> .....	39
<b>5.1.1 Membrane Morphology of PVDF 15% wt. and PVDF 20% wt by SEM-EDS</b> .....	39
<b>5.2 Pore Size</b> .....	45
<b>5.3 FTIR</b> .....	47
<b>5.4 Contact Angle</b> .....	48
<b>5.5. Swelling test</b> .....	50
<b>5.6. Permeability and Rejection</b> .....	51
<b>5.7 Antifouling performance of membrane</b> .....	62
<b>6. Conclusion and Recommendation</b> .....	66
<b>7. Reference</b> .....	68



## List of Figure

Figure 1. Sources of microplastic and nanoplastic [1] .....	12
Figure 2. Size ranges of common contaminants and pore diameters for various separation methods. [5] .....	16
Figure 3. PVDF membrane Fabrication via NIPS Technique [35] .....	17
Figure 4. Asymmetric membrane formation [8].....	21
Figure 5. Schematic diagram of symmetric (b) asymmetric membrane filtration behaviour . [4] .....	22
Figure 6. shows different sizes of microplastics [11] .....	25
Figure 7 Chemical Structure of PVDF [36] .....	27
Figure 8. $\alpha$ , $\beta$ , and $\gamma$ structure PVDF phase [16] .....	27
Figure 9. A schematic diagram of membrane preparation using the NIPS technique.[37] .....	30
Figure 10. (a,b)Components of the Amicon Stirred Cell, schematic of dead-end filtration cell (c). [37] .....	32
Figure 11. Turbidity Tester [37] .....	33
Figure 12. Schematic of a contact angle system featuring a sessile-drop configuration [39] .....	36
Figure 13. Classification of Surface wetting ability by contact angle.[37] .....	37
Figure 14. The advancing and the receding contact angle.[37] .....	37
Figure 15 Surface morphology of PVDF15% wt .....	39
Figure 16. a) EDS spectrum of PVDF15% wt AgNO <sub>3</sub> , b) surface morphology of PVDF15% wt AgNO <sub>3</sub> by SEM.....	40
Figure 17. a) EDS spectrum of PVDF15% wt CuO, b) surface morphology of PVDF15% wt CuO by SEM. ....	40
Figure 18. a) EDS spectrum of PVDF 15% wt TiO <sub>2</sub> , b) surface morphology of PVDF 15% wt TiO <sub>2</sub> by SEM.....	41
Figure 19 Surface morphology of PVDF 20%.....	42
Figure 20. a) EDS spectrum of PVDF 20% AgNO <sub>3</sub> , b) surface morphology of PVDF 20% AgNO <sub>3</sub> by SEM.....	42
Figure 21. a) EDS spectrum of PVDF 20% CuO, b) surface morphology of PVDF 20% CuO by SEM.....	43
Figure 22. EDS spectrum of PVDF 20% TiO <sub>2</sub> b) surface morphology of PVDF 20% TiO <sub>2</sub> by SEM.....	44
Figure 23 FTIR Spectra of PVDF Membranes before and after surface modification .....	47
Figure 24 Permeability and rejection of PVDF 15% wt.....	52
Figure 25 Permeability and rejection of PVDF 15% CuO (run1) .....	52
Figure 26 Permeability and rejection of PVDF 15% CuO (run2) .....	53
Figure 27. Permeability, rejection, and antifouling of PVDF 15% CuO (run3).....	53
Figure 28 Permeability and rejection of PVDF 15% AgNO <sub>3</sub> (run1) .....	54
Figure 29 Permeability and rejection of PVDF 15% wt AgNO <sub>3</sub> (run2) .....	54
Figure 30 Permeability and rejection of PVDF 15% wt AgNO <sub>3</sub> , (run3) .....	54
Figure 31 Permeability and rejection of PVDF 15% wt TiO <sub>2</sub> (run1) .....	55
Figure 32 Permeability and rejection of PVDF 15% wt. TiO <sub>2</sub> (run2) .....	55
Figure 33 Permeability, rejection, and antifouling of PVDF 15% wt. TiO <sub>2</sub> (run3) .....	56
Figure 34 permeability, rejection, of PVDF 20% wt.....	57
Figure 35 Permeability and rejection of PVDF 20% wt CuO (run1).....	57
Figure 36 Permeability and rejection of PVDF 20% wt CuO (run2).....	58

Figure 37 Permeability and rejection of PVDF 20% wt CuO (run3).....	58
Figure 38 Permeability and rejection of PVDF 20% wt AgNO <sub>3</sub> (run1) .....	59
Figure 39 Permeability and rejection of PVDF 20% wt AgNO <sub>3</sub> (run2) .....	59
Figure 40 Permeability and rejection of PVDF 20% wt AgNO <sub>3</sub> (run3) .....	60
Figure 41 Permeability and rejection of PVDF 20% wt TiO <sub>2</sub> (run1) .....	60
Figure 42 Permeability and rejection of PVDF 20% wt TiO <sub>2</sub> (run2) .....	60
Figure 43 Permeability and rejection of PVDF 20% wt TiO <sub>2</sub> (run3) .....	61
Figure 44 Permeability, antifouling of PVDF 15% wt. CuO .....	62
Figure 45 Permeability, antifouling of PVDF 15% wt. AgNO <sub>3</sub> .....	62
Figure 46 Permeability, antifouling of PVDF 15% wt. TiO <sub>2</sub> .....	63
Figure 47 Permeability, antifouling of PVDF 20% wt CuO .....	63
Figure 48 Permeability, antifouling of PVDF 20% wt AgNO <sub>3</sub> .....	64
Figure 49 Permeability, antifouling of PVDF 20% wt TiO <sub>2</sub> .....	64

## List of Table

Table 1. Types of membrane separation and applications [7].....	18
Table 2. Types of polymeric, structure preparation method and their application [7] ...	20
Table 3 Turbidimeters and Their Turbidimetry [19] .....	33
Table 4 pore size measurement of PVDF 15% wt. ....	45
Table 5 Pore size of PVDF 20% wt. ....	45
Table 6 Contact Angle data with images .....	48
Table 7 Water Uptake data in % .....	50
Table 8 Swelling Degree In percentage % .....	50

## List of Equation

Equation 1 Permeability formula .....	34
Equation 2 formula for rejection rate calculation.....	34
Equation 3 Young's equation for contact angle .....	36
Equation 4 Formula for water uptake calculation .....	38
Equation 5 Formula for swelling degree calculation .....	38

## Nomenclature

DI	Distilled water	PSU	Polysulfone
wt%	Weight percentage	PES	polyether sulfone
DMAc	N, N-Dimethylacetamide	PTFE	Polytetrafluoroethylene
DMF	Dimethylformamide	PTFE	Polytetrafluoroethylene
DMSO	Dimethyl sulfoxide	PV	Pervaporation
wt%	Weight percentage	PAN	Polyacrylonitrile
FT-IR	Fourier-transform infrared spectroscopy	PVC	Polyvinyl chloride
WU	Water uptake value	PEST	polyethylene terephthalate
WWTPs	wastewater treatment plants	PVDF	Polyvinylidene Fluoride
MD	Membrane distillation	PVF	Polyvinyl fluoride
MF	Microfiltration	PVP	Polyvinylpyrrolidone
NaCl	Sodium Chloride	CB	Coagulation bath
NaOH	Sodium hydroxide solution	SEM	Scanning electron microscopy
NF	Nanofiltration	TiO <sub>2</sub>	Titanium Dioxide
NIPS	Non-solvent induced phase separation	EDS	Energy Dispersive X-ray Spectroscopy
KOH	potassium hydroxide	MPs	Microplastics
NTUs	Nephelometric turbidity units	NPs	Nanoparticles
PA	Polyamide	UF	Ultrafiltration
PE	Polyethylene	CuO	Copper (II) oxide
PEG	Polyethylene Glycol	PV	pervaporation
PI	Polyimide	PES	Polyethersulfone
PP	Polypropylene	POM	Polyoxymethylene
DAF	Dissolved air flotation	MBR	Membrane Bioreactor
RSF	rapid sand filters	DF	Disc filter
IPA	isopropyl alcohol	AgNO <sub>3</sub>	Silver Nitrate

# 1. Introduction

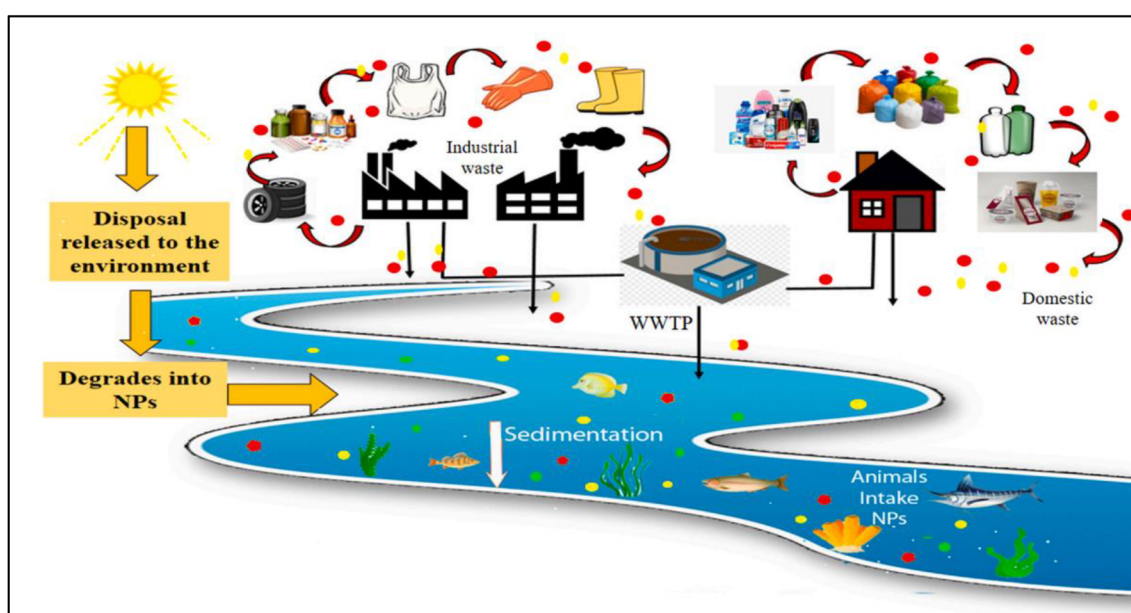
## 1.1 Background and Significance

In contemporary times, the notion of existence without plastics or artificial organic polymers appears inconceivable. Humans rely heavily on plastics, from cosmetics to packaging materials. Moreover, textile industries contribute to water pollution with microplastic contamination. A significant risk of water contamination is the growing number of sectors contaminating water [1,2].

Plastics, or synthetic organic polymers, are becoming widely used worldwide and have largely replaced conventional materials like glass, metal, and wood in various uses. Plastic, used extensively in many different products, is especially prevalent in the packaging industry. Getting raw materials, creating a basic polymer, compounding it into a proper form, and then molding or shaping the plastic are all steps in the manufacturing process. The manufacturing of plastics reached a remarkable 390.7 million metric tons in 2021, an increase of four percent over the previous year. Since the 1950s, there has been a steady increase in the manufacture of plastics, which can be linked to these materials' extraordinary adaptability [2].

The "Plastic Age" is frequently used to describe this period of human history. Plastic is widely used because it is solid and lightweight, making it appropriate for various items. However, plastic waste has a discernible build-up because of the overuse and quick discarding of plastic products. Even the earth's most remote regions are affected by this type of pollution, which includes the surface waters of open oceans [2, 5, and 7].

Based on statistical statistics, Asia is the region that contributes most to the world's plastic production; in 2021, China alone accounted for 32% of the total output. Surprisingly, China has reliably produced six to twelve million metric tons of plastic items monthly in recent years. North America held second in the world plastic manufacturing rankings in 2021, with an 18% share [2]. **Figure 1.** It shows that there are sources of micro and nanoplastic.



*Figure 1. Sources of microplastic and nanoplastic [1]*

Several researchers found that most of the microplastic wastewater comes from textiles; according to Guñdog˘du et al. (2018), fibers made up 60% of the microplastic type found in effluent samples, with film and fragments coming in second and third, respectively. They determined the primary polymeric compositions of microplastics in the effluent to be polyethylene (PE), polyethylene terephthalate (PEST), polyvinyl chloride (PVC), acrylonitrile butadiene styrene, polyoxymethylene (POM), nylon 6, and polypropylene (PP), PEST was the most often seen polymer among them. Because PEST is robust and long-lasting, it is frequently utilized in the textile sector, which means significant levels of PEST microfibers are expected in wastewater (Napper and Thompson 2016). According to a study by Carr et al. (2016), blue and irregular PE particles were the microplastics most often found in wastewater treatment facilities (WWTPs), typically in whitening toothpaste formulations. This suggests that specific types of toothpaste formulations contribute to the presence of microplastics detected in WWTPs [2].

As human civilization develops, water remains essential to all aspects of existence. The world's population has led to a notable increase in the daily generation of large amounts of wastewater from industrial, agricultural, and residential sources. This increase in wastewater is co-occurring as freshwater supplies on Earth must be replenished to meet the increasing demands of an expanding population with increasing water needs [2,4].

The discrepancy between the increasing demand for water and stagnant freshwater reserves has led to an unfair allocation of limited freshwater resources. Diverse industries must compete for this scarce and essential resource, including residential buildings, commercial establishments, and farming operations [7].

This competition has global implications beyond specific industries and affects the fair and sustainable use of water resources worldwide. Initiatives for sustainable water management, conservation techniques, and the creation of cutting-edge water reuse and recycling technologies are frequently used to address this problem [2,3,5,7].

Membrane technology presents a viable way to close the gap between sustainability and affordability. With its potential for little to no chemical use, environmental friendliness, and broad accessibility, it has recently become the go-to option for wastewater treatment procedures [7].

A membrane acts as a hedge by separating and controlling the inflow of specific molecules between two phases. Its structure can be symmetric or asymmetric, homogeneous or miscellaneous, and can take solid or liquid forms. Membranes are put into organic and inorganic groups, depending on what they are made of. Organic membranes are made from synthetic organic polymers used these membranes including polyethylene (PE), polytetrafluoroethylene (PTFE), polypropylene, PVDF, and cellulose acetate, among others, and are primarily used to separate things under pressure, like in microfiltration, ultrafiltration, nanofiltration, and reverse osmosis. Examples of artificial materials in these membranes include plastic, Teflon, and cellulose acetate [3]. Inorganic membranes are made from Ceramics, Metals, Zeolites, and Silica. These barriers are substantial and can handle heat and chemicals without being damaged. They are used in many industries for tasks like separating hydrogen, filtering things at a microscopic scale, and filtering things at a medium scale [2].

Grounded on their properties, membranes can be divided into isotropic and anisotropic kinds. Isotropic membranes have a harmonious physical structure and content. Compared to their porous counterparts, which have lower saturation flux and more minor uses, microporous membranes have comparatively large saturation fluxes; microfiltration operations constantly use microporous isotropic membranes. On the other hand, anisotropic membranes correspond to separate layers with different compositions and topologies and are non-uniform throughout the membrane region. These membranes are exceptionally well suited for reverse osmosis procedures because they have a thin skin above a thicker, largely passable substrate, a membrane whose consistency (thickness) can vary from many hundred micrometers to as little as 10 microns. Further contributing to their suitability for diverse applications [2,3,4]. More information is given in section 2.1.

Effluent from homes and businesses must be treated in wastewater treatment plants (WWTPs) before being recycled or released into rivers. Microplastics (MPs), tiny plastic particles found in water and the environment, are only partially removed by WWTPs despite the efficient removal of many other contaminants. Many of these microplastics escape the purification procedures, endangering aquatic life and thus affecting human health [2].

Membrane filtration stands out as a leading wastewater treatment. Because of its advantages, including its lack of phase shifts or chemical additions, ease of use, and relatively low energy consumption, membrane filtration is a top sustainable wastewater treatment technique [5].

The increasing need for membranes in various industrial processing applications and water and wastewater treatment is driving the expansion of the global membranes market. Tight environmental restrictions and a focus on wastewater treatment are driving factors in the market. Water desalination and growing water shortages are expected to generate growth opportunities in membrane manufacturing, especially in the Asia Pacific, the Middle East & Africa. Regarding application, the membranes market's industrial processing sector is anticipated to expand more quickly than the water and wastewater treatment segment. Membranes find application in diverse industries, such as oil and gas, textiles, pulp and paper, food and beverage, pharmaceuticals, chemical and petrochemicals, and power. This indicates a broad market demand for membranes. The polymeric segment is expected to develop fastest among the different types of membranes. This contains a variety of polymers with high selectivity and ease of use, like polyamides, polyether sulfones, and fluorinated polymers. Compared to ceramic membranes, polymeric membranes are also less expensive. The membrane market size is expected to rise from USD 6.4 billion in 2022 to USD 10.1 billion by 2027 at a compound annual growth rate (CAGR) of 9.7% [2,4].

An optimal membrane should have excellent mechanical properties, permeability, selectivity, and robust thermal and chemical stability. Usually, a combination of elements is required to achieve these desired properties, including high porosity, an exact and narrow pore size distribution, the correct chemical composition, and clearly defined membrane structures, including optimal crystalline forms. The morphologies and structures of the membrane are closely related to the characteristics and performance of PVDF homopolymers. Furthermore, for PVDF copolymers, the chemical makeup is crucial in determining PVDF's crystalline structure and the membrane's general characteristics [4,2].

## 1.2 Scope and limitation

Microplastic filtration is a major challenge for humankind as many factors affect the efficiency and possibilities of filtration. Microplastic contamination has become a major natural issue with far-reaching impacts on environments and open well-being. Imaginative approaches are required to overcome this issue, and membrane-based filtration methods—specifically those that utilize PVDF (polyvinylidene fluoride) films made by the non-solvent initiated stage division (NIPS) technique—offer a practical arrangement. This thesis explores the potential and limitations of microplastic filtration utilizing PVDF films and modification of surface changes using titanium, copper oxide, and silver microparticles and nanoparticles. This consideration aims to decide how well PVDF films channel microplastics from water. The objective of the consideration is to supply an exhaustive understanding of the membrane's capacity to capture microplastic over time by using various concentrations of polymeric material and different particles. The consider takes a shrinking approach to characterizing film chemical and surface properties, looking to determine the conveyance of these properties and their effect on filtration productivity. Changes in NIPS parameters, an essential component of film construction, are examined to see how they influence film structure and, in turn, the viability of microplastic shifting [2,5,41]. In this thesis, the NIPS condition remained unchanged and stable.

The hydrophobic character of PVDF film surfaces is assessed to determine its effect on water intelligence and microplastic grip. This evaluation offers essential data on the membrane's usefulness in energetic natural settings [43].

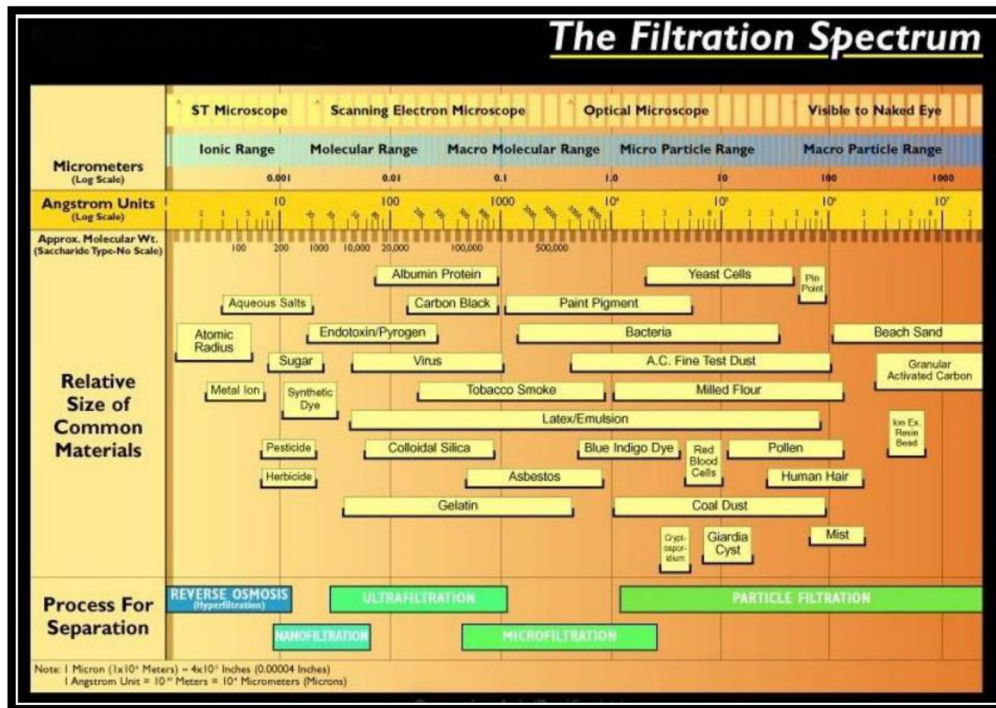
The literature's scope is urgently affected by PVDF films' long-term solidness and fouling resistance amid persistent microplastic sifting. The long-term assessment looks to duplicate real-world circumstances and offer intelligent data on the membrane's versatility for continuous operation. To encourage the increment of the study's biological pertinence, the investigation joins scenarios in which characteristic natural matter is displayed within the water as an implication of interfacing the discoveries with natural conditions [42,43,44].

The scope is extended to incorporate surface changes with micro- and nano-particles of copper, titanium, and silver oxides in a one-of-a-kind way. Even though the study is carried out in carefully directed lab settings, various external elements could affect the film's functionality in real-world circumstances. Some examples are temperature swings, sun exposure, humidity variations, changes in the pH of nearby substances, and additional environmental chemicals or toxins [42, 43, 44].

In summary, porosity, pore size distribution, chemical composition, and customized membrane structures are just a few of the variables that must be carefully considered when designing the perfect membrane. These variables add to improved permeability, selectivity, mechanical strength, and chemical and thermal stability. The interaction of these components is especially significant for PVDF homopolymers and copolymers, where the morphological and compositional features are closely related to the membrane properties [2,5,7].

PVDF is widely used in various process industries because of its exceptional qualities, including its inertness to a broad range of solvents, oils, and acids. PVDF is particularly noteworthy for its wide range of uses in membrane separation processes, including membrane distillation (MD), microfiltration (MF), ultrafiltration (UF), and pervaporation (PV). These membrane-based techniques have significantly impacted resolving pressing environmental

issues, alleviated water scarcity, and improved energy usage [5]. **Figure 2** shows the size of the contaminants and the pore size of various filtration technology spectrums.



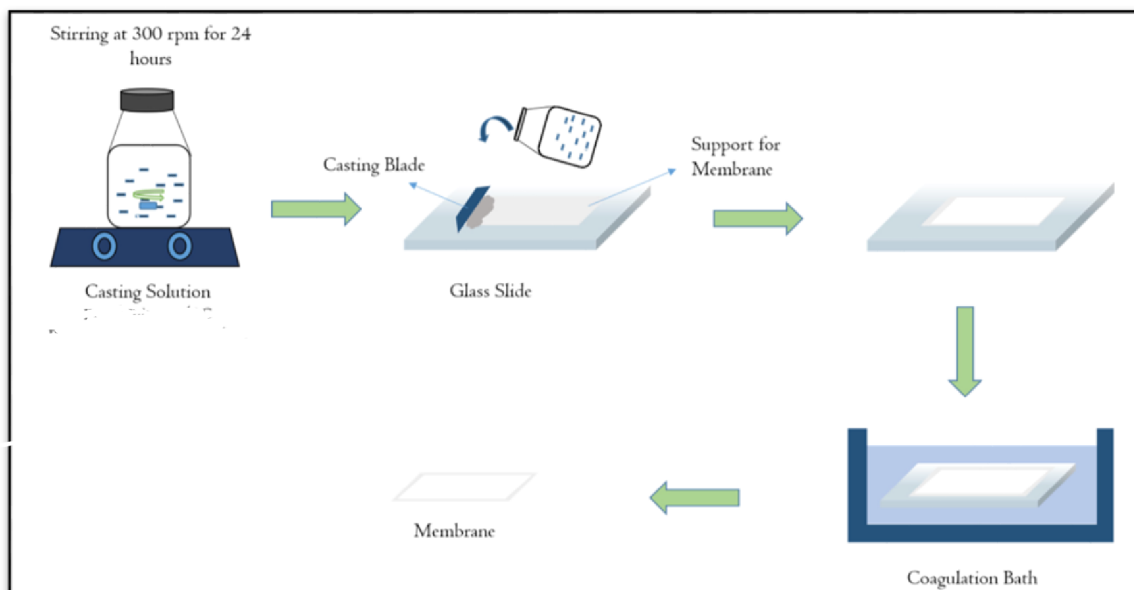
**Figure 2. Size ranges of common contaminants and pore diameters for various separation methods. [5]**

PVDF has excellent qualities that are crucial in improving process efficiency in membrane separation. Its built-in resistance to various oils, solvents, and acids guarantees dependability and longevity under various operating circumstances. The broad availability of PVDF in different molecular weights, offered as pellets and powders, makes it easier to customize membranes to meet fabrication needs, adding to the material's versatility in handling various issues [17,24].

The non-solvent-induced phase separation (NIPS) method is a widely used technology that involves multiple crucial processes to generate flat sheet polymeric membranes. First, some polymeric solution is poured on a support screen and then spread evenly on the desired thickness with a casting knife, which is subsequently added to a bath containing no solvent. Phase inversion, a phenomenon in this environment, causes the polymer to go from a liquid to a solid form. The formation of porous membranes depends on this critical phase inversion.

The inversion process creates porous structures in the membranes by causing the solvent in the polymer solution to migrate outward and into the coagulation bath (CB) and the non-solvent to follow the opposite path. The formation of membranes with asymmetric microstructures results from the phase inversion caused by this complex interchange between solvent and non-solvent [35].





**Figure 3. PVDF membrane Fabrication via NIPS Technique [35]**

The production of microporous PVDF membranes at the laboratory scale using the NIPS technology will be the main emphasis of this thesis. This method guarantees the creation of microporous structures necessary for various applications by enabling the controlled manufacturing of membranes with specific properties. The produced PVDF membranes can be customized to fit the required standards for research and practical goals by adjusting the parameters of the NIPS. **Figure 3** shows the membrane casting via NIPS Technology.

Within the scope of this thesis, the first PVDF solution was prepared with a 15% and 20% wt concentration in DMSO for membrane formation; then, the surface modification was done using three different microparticle nanoparticles for microplastic-contaminated water filtration.

This thesis aims to supply noteworthy commitments to the different fields of microplastic filtration while recognizing the broad run and inherent limitations related to membrane design. The search for information in this region is promising for creating long-term, down-to-earth arrangements for the omnipresent microplastic contamination issue.

## 2. Literature Review

The theoretical part includes a thorough analysis of membrane technology used to remediate wastewater contaminated with microplastics. It covers a detailed examination of polymeric membranes, fouling mitigation techniques, the Non-Solvent-Induced Phase Separation (NIPS) method, and surface changes to improve the membrane's hydrophilicity. The thesis also explores antifouling properties using different types of microparticles and nanoparticles. The focus is on elucidating the intricacies of each aspect to provide a thorough understanding of the critical elements involved in utilizing membrane technology for effective microplastic wastewater treatment [7,8,9].

### 2.1 Membrane Technology in Wastewater Treatment

Several experiments have been done for microplastic removal, as it has been a primary concern worldwide. Membrane technology is classified into two methods: component separation and phase separation. Whereas both component partition and phase separation utilize films in specific settings, they center on distinctive viewpoints of the partition handle. Component division separates components or substances from a blend based on their personal properties. In contrast, phase separation deals with partitioning distinctive stages inside a blend, regularly within the setting of liquid-to-liquid or liquid-gas division. The choice of phrasing depends on the objectives and characteristics of the partition handle beneath the thought [7].

Depending on their appearance, the membranes can be divided into two groups: asymmetric and symmetric. Because the surface layer is skinny, asymmetric membranes filter better than regular separation methods. This performance is better than normal separation, uses less energy than distillation, and does not need extra solvents like extraction processes. Membrane filtration technology is listed below in **Table 1** as Types of polymeric, structure preparation method, and their applications **Table 2**

*Table 1. Types of membrane separation and applications [7]*

<b>Membrane separation</b>	<b>Membrane type</b>	<b>Driving force</b>	<b>Applications</b>
Microfiltration	Symmetric microporous	Hydrostatic pressure	Clarification, sterile filtration
Ultrafiltration	Asymmetric microporous	Hydrostatic pressure	Separation of macromolecular solutions
Nanofiltration	Asymmetric microporous	Hydrostatic pressure	Separation of small organic compounds and selected salts from solutions
Hyperfiltration	Asymmetric composite with homogeneous skin	Hydrostatic pressure	Separation of micro solutes and salts from solutions
Gas permeation	Asymmetric or composite, homogeneous or porous polymer	Hydrostatic pressure, concentration gradient	Separation of gas mixtures

Dialysis	Symmetric microporous	Concentration gradient	Separation of micro solutes and salts from macromolecular solutions
Pervaporation	Asymmetric, composite	Concentration gradient, vapour pressure	Separation of mixtures of volatile liquids
Vapor permeation	Composite	Concentration gradient	Separation of volatile vapors and gases
Membrane distillation	Microporous	Temperature	Separation of water from non-volatile solutes
Electrodialysis	Ion-exchange, homogeneous or microporous polymer	Electrical potential	Separation of ions from water and non-ionic solutes
Electro-osmosis	Microporous charged membrane	Electrical potential	Dewatering of solutions of suspended solids
Electrophoresis	Microfiltration membranes	Electrical potential, hydrostatic pressure	Separation of water and ions from colloidal solutions
Liquid membranes	The microporous, liquid carrier	Concentration, reaction	Separation of ions and solutes from aqueous solutions

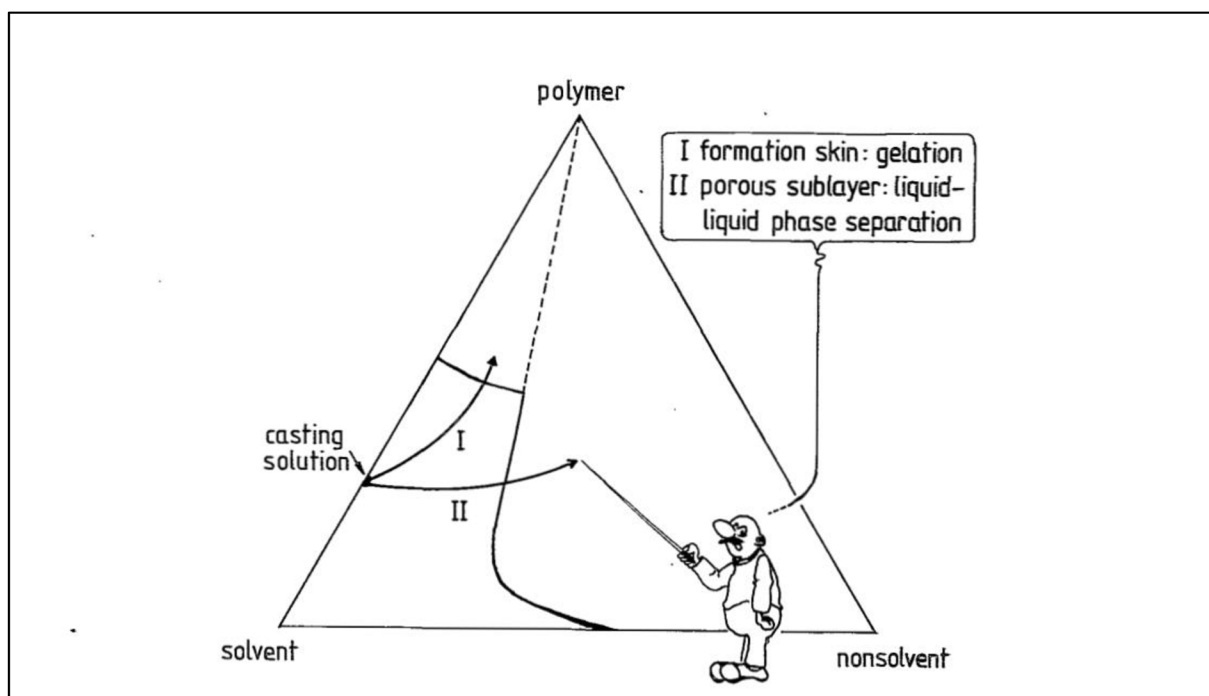
**Table 2. Types of polymeric, structure preparation method, and their application [7]**

<b>Membrane type</b>	<b>Membrane structure</b>	<b>Preparation</b>	<b>Applications</b>
Asymmetric CA, PA, PS, PAN	Homogeneous or microporous, 'skin' on a microporous substructure	Casting and precipitation	UF and RO (MF) GP, PV
Composite CA, PA, PS, PI	Homogeneous polymer film on a microporous substructure	Deposition on microporous substructure	RO, GP, PV
Homogeneous S	Homogeneous polymer film	Extrusion	GP
Ion exchange DVB, PTFE	Homogeneous or micro-porous copolymer a film with positive or negatively charged fixed ions	Immersion of ion-exchange powder in polymer, or sulphonation and amination of homogeneous polymer film	ED
Microporous: ceramic, metal	0.05-20 um pore diameter	Moulding and sintering	GP
Glass	10-100 um pore diameter	Leaching from a two-component glass mixture	F (molecular mixtures)
Microporous: sintered polymer PTFE, PE, PP	0.1-20 um pore diameter	Moulding and sintering	F (suspensions, air filtration)
Microporous: stretched polymer PTFE, PE	0.1-5 um pore diameter	Stretching a partial crystalline film	F (air, organic solvents)
Microporous: Track-etched PC, PEsT	0.02-20 um pore diameter	Irradiation and acid leaching	F (suspensions, sterile filtration)
Symmetric micro-porous phase inversion CA	0.1-10 um pore diameter	Casting and precipitation	Sterile filtration, water purification dialysis

### 2.1.1 Asymmetric membrane

Asymmetric membranes are necessary for pressure-driven operations such as reverse osmosis and ultrafiltration. They comprise a very porous sublayer that is one hundred–200  $\mu\text{m}$  thick and sits on top of an extremely thin (0.1–2  $\mu\text{m}$ ) polymer layer. In pressure-driven processes, the sublayer only provides support and does not affect separation properties or filtration rates. Reverse osmosis and ultrafiltration technologies exhibit an inverse relationship between the filtration rate and barrier layer thickness. The illustrated image below in **Figure 4** shows that asymmetric membrane formation has more excellent filtration rates for materials with comparable thickness [7,8].

Asymmetric membranes offer yet another noteworthy benefit. Conventional symmetric structures operate as depth filters and hold most particles within their internal structure. When used, the flux decreases due to the membrane plugged by these trapped particles. Surface filters, known as asymmetric membranes, hold all rejected materials at the surface where they are retained. The shear forces generated by the feed solution traveling parallel to the membrane surface can eliminate them [7,8].



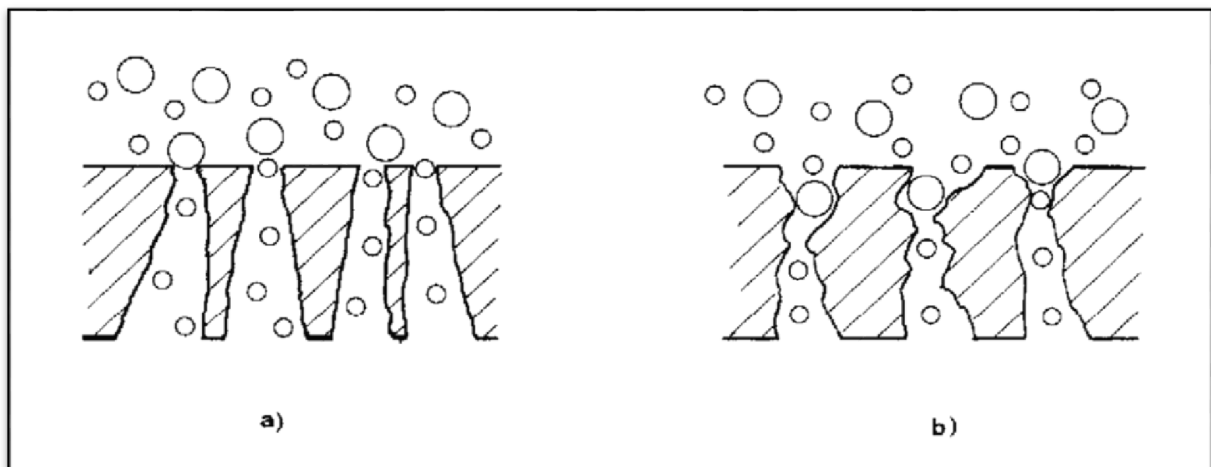
**Figure 4. Asymmetric membrane formation [8]**

Some researchers argue that membrane asymmetry is present in the cast film of concentrated polymer solutions even before precipitation and that other processing processes reinforce the asymmetry. Prominent proponents of this position are Panar and Tanny. [8] A different faction contends that evaporation in the cast film's upper layer causes skin development. Some other proponents of this viewpoint include Sourirajan, Kunst, Kesting, and Anderson [9]. They assert that the length and circumstances of the evaporation process significantly impact the membrane's characteristics. An opposing viewpoint states that phase separation and diffusional processes interact intricately to determine membrane asymmetry, with the coagulation process as the main driver. Scholars such as Frommer, Strathmann, and Koen hen contribute significantly to this viewpoint [6].

Nevertheless, the poll reveals divergent views on the requirement of solvent evaporation. Some suggest that it is possible to manufacture high-quality asymmetric membranes without extensive solvent evaporation, mentioning systems like cellulose acetate/dioxane/water and Poly-sulfone/DMF/water as examples [4,8]. Successful examples of air-free membrane construction, such as Strathmann's asymmetric hollow fibres, cast doubt on the idea that evaporation is a stage that is always necessary. However, the study admits that evaporation might be advantageous in certain situations. The degree to which structure forms in the casting solution depends on the thermodynamics of the polymer-solvent/nonsolvent combination. Therefore, the choice of solvents and nonsolvent must be made carefully [8].

The authors emphasize the importance of investigating the coagulation process to understand how asymmetric structures form. They argue that nonsolvent is essential to creating structures and affects the characteristics of membranes. Therefore, carefully analysing the mechanisms involved in the coagulation step of membrane creation should yield fundamental insights into the formation of asymmetric structures [6,8,9].

**Figure 5** shows the Schematic diagram of symmetric and asymmetric membrane filtration behavior.



*Figure 5. Schematic diagram of symmetric (b) asymmetric membrane filtration behaviour. [4]*

### 2.1.2 Membrane Process for Microplastic Removal

It is crucial to stress that, given the variety of wastewater compositions that need to be treated, evaluating the literature's data on the effectiveness of microplastic removal is challenging. It is crucial to comprehend the significance of microplastic (MP) size, as numerous studies indicate that although membrane filtration removes a significant amount of microplastics, the amount removed can vary depending on the microplastics' characteristics. Microplastics have been shown in several studies to cause considerable membrane fouling during the filtration process [11,5]. According to several studies, the sizes of MP cause membrane fouling as well, so it is essential to enhance the performance of membrane fouling. Several investigations have identified critical factors for effective microplastic filtration, including microplastic mass, size, shape, chemical composition, and concentration considerations. The efficiency of filtration is influenced by various factors in the membrane process, such as membrane material, pore size, thickness, and surface properties. Additionally, the source of water and membrane process

parameters, including filter efficiency, flux, pressure, and rejection/removal, also play a significant role in determining the overall effectiveness of microplastic filtration[11].

Studies have explored methods to improve membrane fouling performance [11,12,13]; many of these studies have concentrated on using amine treatment and incorporating nanoparticles to increase the hydrophilicity and anti-fouling properties of membranes; this antifouling property enhances the filtration performance of membranes. These studies have used a range of membrane filtering techniques [13]. Numerous experiments have been conducted employing different polymers and sizes to understand the parameters affecting filter performance. All this research points to the fact that filtration efficiency depends on several variables, including MP size, characteristics, and technique [10,12,13]. As per several studies on various aspects of microplastics (size, property, sources), a research investigation reported on several microplastic filtration methods concludes that the literature review highlights the need to create specialized microplastic treatment techniques to reduce plastic pollution[11,12,13]. Now, wastewater treatment facilities and the water sector lack the knowledge and equipment to remove microplastics from wastewater efficiently. According to several studies, effective tertiary treatment is needed to remove plastic from sewage. With a 99.9% microplastic removal effectiveness, membrane processes—specifically, membrane bioreactors or MBRs (membrane bioreactors)—show much potential among these tertiary processes. MBRs also offer the chance to reduce the number of process stages in wastewater treatment plants. To further assure more effective removal from effluents, a more thorough and uniform chemical-physical characterization of plastic is essential for choosing appropriate techniques. [11,12].

The literature underlines the necessity of characterizing even nanoplastics, which may have more severe biological implications. It underscores the difficulties in comparing results because no standard characterization techniques exist. Implementing an environmental pollution awareness policy to reduce single-use plastic materials and developing operational procedures and production based on biodegradable materials to prevent environmental accumulation are complementary but constructive measures for reducing microplastic pollution [11].

As we need more understanding and advanced technology to deal with wastewater treatment, Scientists Talvitie et al. [13] from universities in Finland improve their understanding of microplastic contamination in the environment from domestic wash [13]. On the other hand, the second study done by Pirc et al. [12], which was published on 22 September 2016 [12], aimed to facilitate an estimate of the total mass of fibers released into the environment from this specific source, the study's goal was to collect fresh mass-based data regarding the release of fibers during the washing of a typical textile. They also looked into how this discharge is affected by using laundry detergent and softener [12].

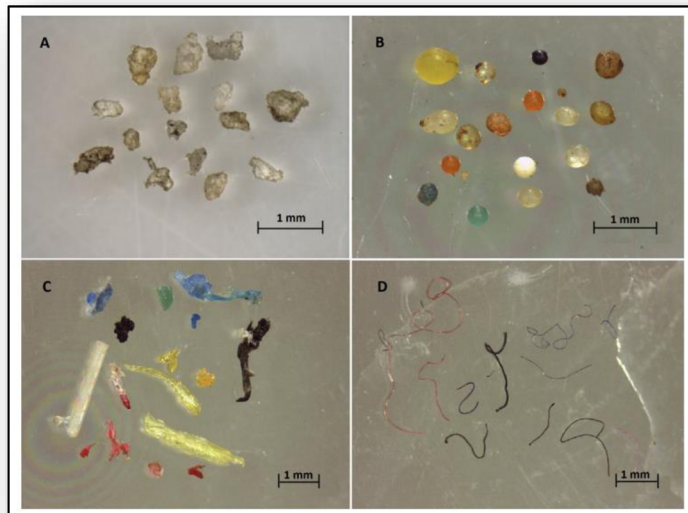
A research study by Talvitie et al. [13] investigated various cutting-edge wastewater treatment technologies for use in WWTPs. Dissolved air flotation (DAF), rapid (gravity) sand filters (RSF), micro-screen filtration with disc filters (DF), and a pilot membrane bioreactor (MBR) unit were among the tertiary treatment methods that have been examined. Notably, Paroinen WWTP in Hameenlinna used DAF, Kenkaveronniemi WWTP in Mikkeli deployed a prototype MBR unit, Kakolanmaki WWTP in Turku used quicksand filters, and Viikinmaki WWTP in Helsinki used a pilot-scale disc filter for micro-screen filtering. The study aimed to evaluate how well these cutting-edge treatment techniques—each with unique qualities—removed

contaminants from wastewater [13]. The results enhance the knowledge of the efficiency and efficacy of contemporary wastewater treatment technology and expand on their potential applications in mitigating environmental pollution [13].

The study by Talvitie et al.[13] aimed to evaluate the efficiency of cutting-edge wastewater treatment technologies in removing microplastics (MPs) from effluent.[13] These technologies include membrane bioreactors (MBR), dissolved air flotation (DAF), rapid sand filters (RSF), and disc filters (DF). The most effective method for notably lowering MP concentrations was MBR. The study addressed issues with MP analysis and underlined the value of regular operating procedures. The success of various treatment modalities in eliminating all MP size fractions highlights the importance of the last stages of treatment for more minor MPs. This study identified different polymer types, most notably polyester (PES), for accurate MP assessment in effluents and suggested large-volume sampling and in-situ pumping.[13] Estimates of primary and secondary MP proportions helped with mitigation plans by providing information about possible sources. For microbeads and textile fibers, distinguishing between primary and secondary MPs is essential for locating sources and putting targeted solutions in place. The study improves our knowledge of MP removal efficiency in wastewater treatment and emphasizes the continuous necessity for trustworthy analytical techniques [13].

This study by Talvitie et al [13] demonstrated how well-suited modern wastewater treatment technologies eliminate microplastics (>20 mm) from primary and secondary effluents. In particular, the Membrane Bioreactor (MBR) is one such technology. Significant removal rates were also demonstrated by other treatments, such as disc filter (DF), dissolved air flotation (DAF), and rapid sand filters (RSF). The investigation identified Thirteen polymer kinds, with polyester (PES) and polyethylene (PE) making up the majority. It is essential to comprehend the origins of microplastics, such as synthetic fibers and beads, to develop treatment plans that effectively address aquatic contamination [13]. This study used different microplastic sources, shown in **Figure 6**. The study highlighted the intricacies of microplastic removal, focusing on things such as membrane properties, water source, and process parameters. It also stressed the need for specialized microplastic management techniques, such as Membrane Bioreactors (MBRs), which provide a promising option for tertiary treatment. This study exclusively examined modern wastewater treatment technologies like MBRs, dissolved air flotation (DAF), rapid sand filter (RSF), and disc filter (DF) used by different wastewater treatment plants. The results showed that MBR was the best at lowering MP concentrations, thus suggesting the importance of having consistent operating procedures and precise analytical techniques [13].





**Figure 6. shows different sizes of microplastics [11]**

#### Challenges and Factors Affecting Filtration:

Both studies by Talvitie et al [13] and U. Pirc et. al [12] mentioned the problems of membrane fouling and the effects of factors such as microplastic shape, size, or concentration Pirc et. Al [12] pointed out that adhering to standard operating procedures and using correct analysis methods is essential[12].

Pirc et al. [12] investigated were helpful in understand how microplastic emissions domestically affect the environment, and how it investigates fiber release during washing, focusing on polyester fleece blankets. They utilized various analytical techniques to identify the fabric composition and conducted washing trials with and without additives. Results showed varied initial fiber release, stabilizing over subsequent cycles. Additives had minimal impact. The study also assessed filtering system effectiveness and estimated annual fiber emissions per person, emphasizing the significant contribution of home textile washing to microfiber pollution. Their findings underscore the need for further research and mitigation efforts. Additionally, the study offers valuable insights for evaluating cumulative microplastic emissions [12].

## 2.2 Polymers Used in Membrane Technology

The choice of polymers in membrane technology is guided by their unique features, which are consistent with the requirements for making a membrane and their respective application fields. Various natural biopolymers and synthetic polymers are used for membrane formation[15,23].

Several cellulose polymers, such as cellulose acetate (CA), are essential cellulose acquired because of their varied applications and distinctive features, such as their hydrophilic property biodegradability. Sourced from all-natural sources coupled with eco-friendly resources, CA flaunts considerable benefits such as reduced poisoning and biodegradability. CA has biocompatibility; it is also known for its low fouling tendency. CA has a significant role in modern membrane technology, specifically in water associated with wastewater therapy, and holds substantial value. CA membrane layers are favored over polymers for their desirable

hydrophilic attributes, cost-effectiveness, and sustainability. Cellulose is utilized in the production of macro, nano, and chemically modified forms of membranes known as cellulose by-products and is used for ultrafiltration, microfiltration, and gas separation [23].

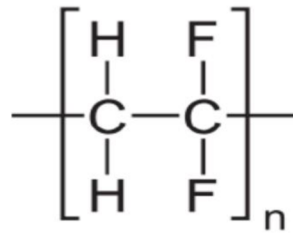
Several synthetic polymers are also used for membrane technology [10,15].

- Polyamide (PA): Polyamides have good mechanical strength and chemical resistance, and this polymer used in membrane layer innovation is typically artificial and consists of products like thin-film compound membrane layers utilized in reverse osmosis.
- Polysulfone (PSU)/polyether sulfone (PES): This synthetic polymer is often used in ultrafiltration and microfiltration membranes (water and wastewater treatment) because of its chemical resistance, thermal security, and mechanical strength.
- Polypropylene (PP)/polyethylene (PE): These polymers often fabricate porous membranes in microfiltration and ultrafiltration membranes because of their low cost and chemical resistance.
- Polytetrafluoroethylene (PTFE): PTFE is an artificial fluoropolymer used in different membrane layer applications because of its chemical resistance, nonstick, hydrophobic nature, and excellent temperature resistance.
- Polyimide (PI): Polyimides are artificial polymers that use gas-splitting up membrane layers due to their heat security plus exceptional obstacle residential properties.
- Polyetherimide (PEI): PEI is an artificial polymer in gas-split-up membranes.
- Poly(ether-block-amide) (PEBA): PEBA is an artificial polymer that uses gas splitting up membrane layers and occasionally in water filtration membrane layers.
- Polyacrylonitrile (PAN): PAN is an artificial polymer manufacturing hollow fiber membrane layers for ultra-filtration.

Among all polymers, PVDF is a widely used polymer. PVDF is a semicrystalline polymer. It has four different crystalline forms that are represented by the letters  $\alpha$ ,  $\beta$ ,  $\gamma$ , and  $\delta$ . These structures result from differences in the polymer chains' conformations inside the PVDF substance. The most common and stable form of PVDF is the  $\alpha$ -phase. The polymer chains in this structure take on an all-trans conformation, and the  $\alpha$ -phase is distinguished by an extraordinarily symmetrical arrangement of the chains. This phase usually gives PVDF good mechanical strength and chemical resistance; the  $\beta$ -phase introduces rotational disorder in the polymer chains, making it less symmetrical than the  $\alpha$ -phase. It also partially rotates some carbon-fluorine bonds, producing a less regular chain conformation. PVDF in the  $\beta$ -phase could have improved piezoelectric characteristics, which would be helpful for actuators and sensors, among other uses. The polymer chains' helical shape characterizes the  $\gamma$ -phase. Compared to the  $\alpha$ -phase, this phase is linked to a lower energy state and introduces a helical symmetry. PVDF in the  $\gamma$ -phase may have unique optical qualities and enhanced flexibility, which makes it appropriate for ferroelectric devices and other specific uses. A fourth, less frequently observed  $\delta$ -phase features tilted chains and a non-centrosymmetric structure [16,24,47]. This polymer is highly resistant to fouling. Due to this, it can operate in a wide range of temperatures [15].

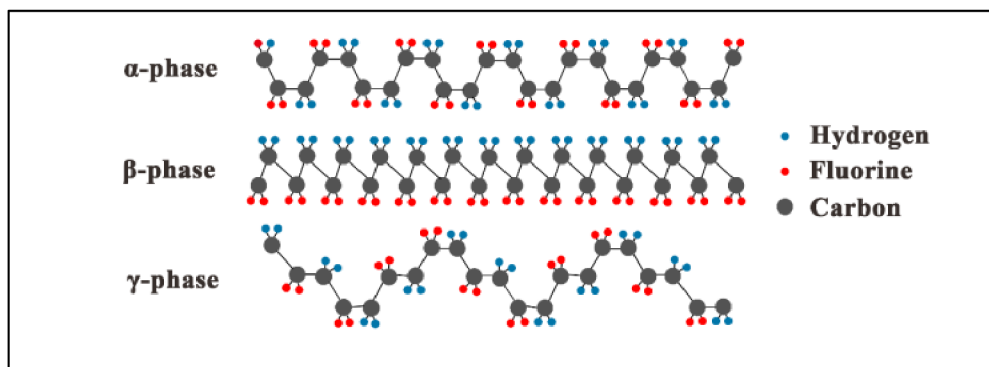
PVDF usually consists of 59.4 wt. % fluorine and 3.0 wt. % hydrogen [15]. PVDF is commonly produced via solution or suspension polymerization techniques, employing free radical initiators to form the structural unit of  $-\text{CH}_2\text{-CF}_2-$ , as depicted in **Figure 7**. The unique

residential properties of PVDF, emerging from its crystalline framework, are affected by the spatial plan of CH<sub>2</sub> and CF<sub>2</sub> teams along the polymer chains[14].



**Figure 7 Chemical Structure of PVDF [36]**

The development and preparation of PVDF membranes are guided by the distinctive properties of its amorphous and crystalline phases. While the amorphous phase contributes flexibility and significant mechanical properties, the crystalline phase offers thermal and chemical resistance, antifouling properties, UV radiation protection, and natural non-adsorption characteristics [16,24]. Despite PVDF's drawbacks, such as hydrophobicity, reduced porosity, and limited functional groups, its hydrophilicity can be enhanced through solvent selection during membrane preparation [14,15]. Hydrophilicity and fouling resistance are crucial considerations, with efforts focused on modifying crystalline polymorphous frameworks to optimize membrane properties [14,15,24]. Polymer crystallinity significantly influences membrane mechanical strength and resistance, with  $\alpha$  and  $\beta$  PVDF phases commonly utilized, particularly in membranes produced via the NIPS method [14,15]. The  $\alpha$ -PVDF phase, characterized by trans-gauche (TGTG') chains forming non-polar chains, facilitates easy pollutant transfer through hydrophobic interactions on the membrane surface [15,16,24]. The  $\beta$ -PVDF phase, derived from the  $\alpha$ -PVDF stage through various methods, features planar zigzag (TTTT) chains and exhibits stronger interactions with polarized particles, contributing to enhanced anti-fouling properties, **Figure 8** Shows PVDF's  $\alpha$ ,  $\beta$ , and  $\gamma$  structure. These structural features and interactions are vital in membrane preparation, guiding solvent selection, crystallinity modification, and overall membrane design to optimize application performance [15,16,24].



**Figure 8.  $\alpha$ ,  $\beta$ , and  $\gamma$  structure PVDF phase [16]**

### 3. Aim of the thesis

Water scarcity is a significant global concern due to population growth, urbanization, climate change, and ineffective water management practices. As the demand for freshwater resources escalates, many regions face water stress or scarcity, posing substantial social, economic, and environmental challenges [40]. currently, plastic pollution is pervasive, with reports indicating its rapid dissemination across diverse geographical locations, marine environments, and biological organisms. The increasing worldwide manufacture of plastics, which amounted to 360 million metric tons in 2018, worsens this issue [41]. While a hypothesis suggests the accumulation of microplastics within subtropical gyres, the mechanisms governing their movement and transport within the ocean, especially along the vertical axis, remain largely elusive. The ingestion of microplastics by organisms poses risks of physical harm, such as internal abrasions and obstructions. Despite the plausible population-level impacts, our understanding of these consequences remains rudimentary. Consequently, further research is imperative to comprehensively evaluate the ecological ramifications of microplastic pollution in marine ecosystems [40].

This study aims to develop a fouling-resistant membrane by using micro and nano-particles for surface modification of the membrane, which is capable of achieving high membrane permeability and effectively rejecting microplastics from microplastic-contaminated water. The characterization of the membrane will involve several techniques, including SEM-EDS, FT-IR (Fourier-transform infrared spectroscopy), filtration devices for permeability and rejection measurement, water uptake and swelling tests, porosity analysis, and water contact angle measurements.

Anticipated outcomes include the development of a PVDF microporous membrane with enhanced fouling resistance prepared via the Non-Solvent Induced Phase Separation (NIPS) technique. Furthermore, the study aims to compare the permeability and rejection performance between PVDF 15% wt and PVDF 20% wt. with their modification. The expected results include achieving high membrane permeability and effective rejection of microplastics, thus demonstrating the efficacy of the developed membrane for water filtration applications

## 4 Materials, Equipment & Method

### 4.1 Material selection

The effective removal of microplastics poses a considerable challenge in contemporary environmental research. The material selection, preparation, and filtration method we chose majorly impacts filter efficiency regarding flux and rejection of pollutants.

Polyvinylidene fluoride (PVDF) has been identified as a suitable polymer for preparing polymeric membranes utilized for microplastic separation [37]. PVDF polymeric membrane prepared with 15% and 20% concentrations, along with nanoparticles such as AgNO<sub>3</sub>, TiO<sub>2</sub>, and microparticle CuO, have been employed for surface modification to augment surface hydrophilicity and mitigate membrane fouling; these particles exhibit antibacterial and antifouling properties based on the used amount [42,43,44].

As the polymer material, PVDF powder (density  $\rho = 1.78 \text{ g cm}^{-3}$ ) was selected and provided by Arkema, France.

N, N-Dimethylacetamide (DMAc) (molar mass  $M = 87,12 \text{ g/mol}$ ,  $\rho = 0,937 \text{ g cm}^{-3}$  / at 25°C) was used as the solvent in membrane preparation and provided by Penta Chemicals Unlimited.

For surface modification, silver nitrate (AgNO<sub>3</sub>) and Copper oxide (CuO) were purchased from Penta Chemical Unlimited. Titanium dioxide (TiO<sub>2</sub>) was purchased from Sigma Aldrich.

To prepare an alkali solution, Chemical Unlimited purchased KOH (potassium hydroxide pellets A.G) and isopropyl alcohol (IPA) p.a.

Ascorbic Acid was employed as a reducing agent for AgNO<sub>3</sub>. The reaction between AgNO<sub>3</sub> and the ascorbic acid produces monodisperse ultrafine silver powder [45]. The membrane with AgNO<sub>3</sub> was immersed in ascorbic acid for 24 hours.

### 4.2 Material and membrane Preparation

Polyvinylidene fluoride (PVDF) powder was blended with N, N-Dimethylacetamide (DMAc) solvent in two concentrations (15% and 20% wt) to formulate the polymeric solution. The mixture underwent magnetic stirring for 24 hours at 400 rpm using the Hei Dolph Company's Magnetic Stirrer, and after completely dissolving the polymer at 60°C, a homogeneous and dense polymeric solution was obtained.

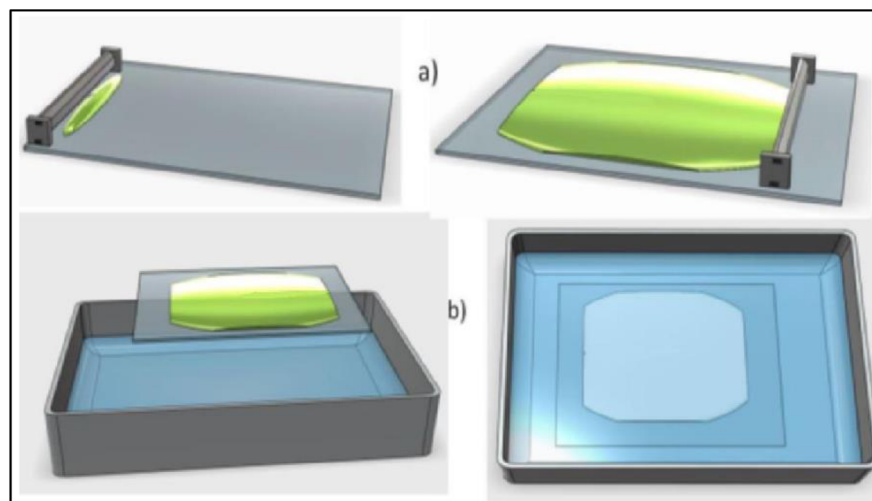
The dope solution was allowed to degas overnight to eliminate any apparent gas bubbles. The prepared solution was film then taken for casting from thin-film membranes.

Subsequently, the nanoparticle and microparticle solutions for surface modification were prepared. AgNO<sub>3</sub> 0.25g with 50 m.L D.I water, CuO with 50 m.L of D.I water, and TiO<sub>2</sub> with 50 m.L of water were prepared. All particles were mixed in solvent for 2 hours. To avoid aggregation, the solution was kept in an ultrasonic bath. Subsequently, an alkali solution (5grams of KOH) was dissolved in 50 m.L of IPA

All nanoparticle and microparticle solutions underwent stirring on the Hei Dolph Company's Magnetic Stirrer for 2 hours to ensure proper mixing. An alkali solution was also prepared by dissolving 5gm of potassium hydroxide (KOH) in 50 ml. of isopropyl alcohol (IPA).

The flat sheet membrane fabrication process utilizing PVDF polymeric solutions with 15% and 20% wt in NIPS (non-solvent-induced phase separation) method was conducted on a laboratory scale following a systematic procedure:

1. The PVDF dope solution is uniformly applied onto a glass plate and manually cast to achieve a predetermined thickness of 200  $\mu\text{m}$  using a casting blade (VF1502-448 – TQC sheen).
2. The glass plate layered spread dope solution was immersed in deionized (D.I.) water for 15 minutes to swap the DMAc solvent entirely. The bath, including the glass plate, was kept at room temperature. Following the 15-minute immersion period, a membrane with an uneven microstructure thin film was obtained. The graphical illustration is shown below in **Figure 9**.
3. After the phase inversion process, the membrane was carefully removed from the glass plate and placed in a container filled with D.I. water in wet condition until testing with a filtration unit.
4. After the membrane formation with PVDF 15% wt and PVDF 20%wt solutions, a feed solution was prepared for filter testing by introducing 0.4 ml. (0.008% concentration) of microplastic particles with a size of 0.5  $\mu\text{m}$  into 500 ml. of deionized water. The solution was thoroughly mixed by agitation for several minutes to ensure homogeneity

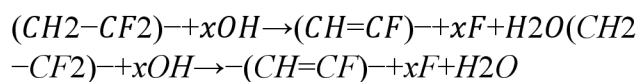


*Figure 9. A schematic diagram of membrane preparation using the NIPS technique. [37]*

### 4.3 Surface Modification of Membrane

After the preparation of the film, the subsequent step entails implementing the surface modification procedure. First, a chemical alkaline treatment is employed to alter the surface of the membrane to incorporate hydroxyl groups into the PVDF surface. Subsequently, specific nanoparticles (NPs) and microparticles (MPs), including nanoparticle  $\text{TiO}_2$ , microparticle  $\text{CuO}$ , and nanoparticle  $\text{AgNO}_3$ , are chosen and affixed onto the membrane surface to augment hydrophilicity and mitigate membrane fouling. The laboratory-scale process is defined as follows:

1. PVDF membranes with 15% and 20% concentrations are immersed in an alkaline solution for 30 minutes. The chemical reaction involved in the alkaline solution treatment is represented as:



Where  $x$  represents  $K$  [17].

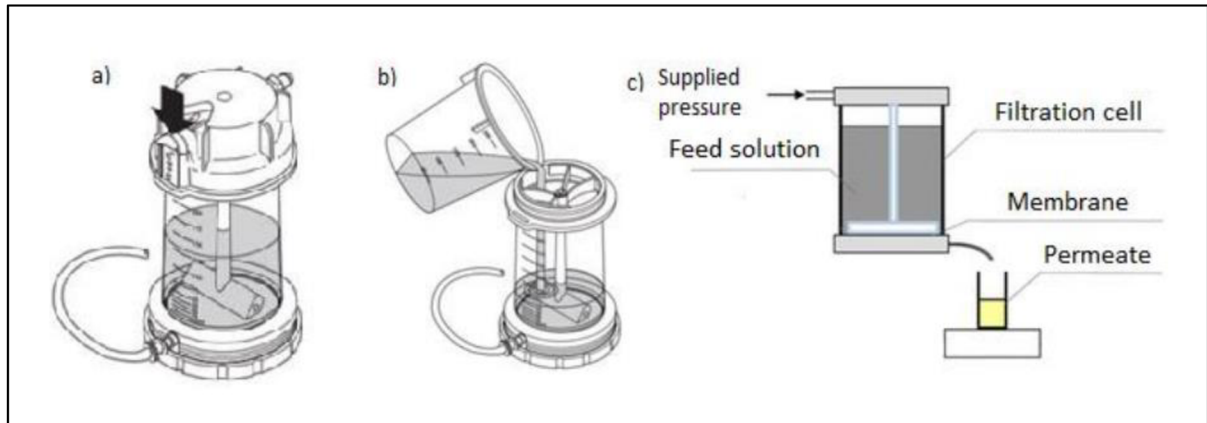
2. After removing from the alkaline solution, the membranes are rinsed with deionized (D.I.) water. Subsequently, the treated membrane samples are individually immersed in separate glass beakers containing nanoparticle  $\text{AgNO}_3$ ,  $\text{TiO}_2$ , and microparticle  $\text{CuO}$  solutions for 24 hours.
3. Upon the 24-hour immersion, the membranes are extracted from the nanoparticle and microparticle solutions and subjected to multiple rinses with D.I. water to eliminate any excess nanoparticles adhering to the membrane surface. The successful incorporation of nanoparticles onto the membrane surface is observed to enhance hydrophilicity, antifouling properties, and permeability.
4. Following successful surface modification, the PVDF membranes with nanoparticles  $\text{AgNO}_3$  incorporated at 15% and 20% concentrations undergo immersion in ascorbic acid for an additional 24-hour duration to reduce  $\text{AgNO}_3$  and form silver nanoparticles.

### 4.4 Filtration Test

The filtration was performed using an Amicon dead-end device (Amicon stirred cell model 8050, 50ml, UFSC05001).

Before insertion into the Amicon dead-end filter, circular membranes with a diameter of 4.45 cm underwent meticulous cutting and cleaning procedures using deionized (DI) water. Subsequently, the Amicon lid was affixed to a pressure supply, and the Amicon cell was filled with a total volume of 50 ml. of feed solutions (microplastics DI water).

Following the pressure within the system, it was precisely adjusted to 0.75 Bar. A graphical representation of this experimental setup is provided in **Figure 10**.



**Figure 10. (a,b) Components of the Amicon Stirred Cell, schematic of dead-end filtration cell (c). [37]**

In This experimental setup, circular membranes with an effective filtration area of 13.4 cm<sup>2</sup> filter the respective filtering solutions (microplastic solution prepared for filter test). The collection time of permeated fluid in increments of 10 mL, 20 mL, 30 mL, and 40 mL. was meticulously recorded for subsequent analysis. Following each filtration test, the collected filtered solution underwent turbidity testing. Since a greater rejection rate indicates better filtering performance, turbidity rejection rate demonstrates the quality of membrane filtration character. This filtration procedure was repeated thrice for each sample. (After each test, the membrane was washed thoroughly with DI water to remove microplastic particles adhered to the membrane surface). The collected filtered wastewater was subjected to turbidity testing using a turbidimeter.

#### 4.5 Turbidity Test

This research study used a turbidimeter to calculate the turbidity rejection rate, which indicates the membrane's filtering efficiency. A higher rejection rate signifies superior filtering performance, thus indicating the membrane's capability to separate particles effectively.

Instead of quantifying the number of suspended particles in the water, turbidity indicates how much they affect the light's scattering and weakening. This shows how transparent the water is. Greater turbidity values are correlated with higher degrees of dispersed or weaker light intensity [20].

Several instruments can be used for the turbidity test measurement [19,20]. The instrument name and their unit are given below in **Table 3**.



*Table 3 Turbidimeters and Their Turbidimetry [19]*

Instrument Design	Reporting Unit
Nephelometric non-ratio turbidimeters	(NTU)
Ratio White Light turbidimeters	(NTRU)
Nephelometric, near-IR turbidimeters, non-ratiometric	(FNU)
Nephelometric near-IR turbidimeters, ratio metric	(FNRU)
Surface Scatter turbidimeters	(SSU)
Formazin Back Scatter Unit	(FBU)
Backscatter Unit	(BU)
Formazin attenuation Unit	(FAU)
Light attenuation Unit	(AU)
Nephelometric Turbidity Multibeam Unit	(NTMU)

In the present research, the turbidity was measured with the Lovibond Turbidimeter TB300 IR model. The tested solutions were put into a cuvette placed within the measurement chamber. The turbidimeter was then used to measure the turbidity in NTUs. The turbidity tester used in this study is represented in **Figure 11**.



*Figure 11. Turbidity Tester [37]*

#### **4.6 Permeability and Rejection**

Permeability is the fundamental physical attribute of porous materials, while porosity represents their primary geometric feature. While porosity gauges a material's capacity to retain fluids, permeability characterizes the porous medium's capability to allow fluid flow. Permeability indicates the ease of liquid movement through a porous material and provides insights into the size of membrane pores and the connectivity of void spaces within it. Calculating permeability and elucidating the relationship between fluid flow and porous media properties often entails applying Darcy's Law [21,22].

The water flow of porous membrane experiments was measured under ambient settings with a dead-end filtering device powered by pressure, and permeability was calculated using the formula below (**Eqn. 1**).

**Equation 1 Permeability formula**

$$k = \frac{L}{AtP} \quad (\text{L}/(\text{m}^2\text{hbar}))$$

k is permeability,  
 L is the amount of permeate at a specific time  
 A is the area of the membrane  
 t is the time of collected permeate at specific intervals  
 P is the applied pressure.

An indicator of the membrane filtration performance is the membrane rejection rate; a greater rejection rate denotes better filtering performance. This measure evaluates a selected membrane's performance in particle separation procedures. The following formula is used to calculate the rejection rate. The formula is given below (**Eqn. 2**).

**Equation 2 formula for rejection rate calculation**

$$\text{Particle rejection rate} = \frac{T_{\text{initial feed solution}} - T_{\text{permeate solution}}}{T_{\text{initial feed solution}}} \times 100\%$$

- Rate of rejection of particles (unit in percentage, %)
- *T<sub>initial feed solution</sub>* (unit in nephelometric turbidity units, NTUs) denoted for turbidity of initial feed solution of filtration test.
- *T<sub>permeate solution</sub>* (unit in nephelometric turbidity units, NTUs) denoted for turbidity of permeate solution of filtration test.

**4.7 Membrane Characterization**

Water contact angle, membrane filtration performance (permeability and rejection), water absorption, and swelling degree. A scanning electron microscope (SEM-EDS) and ImageJ software. Fourier transform infrared spectroscopy (FTIR – Nicolet iZ10) was also used to determine the chemical contents of the membranes. Simultaneously, the experiment on micropollutant separation offered valuable information regarding the filtration capabilities of the chosen casting membranes.

**4.7.1 Fourier transformed infrared Spectroscopy**

Fourier Transform Infrared Spectroscopy (FTIR) is a fundamental analytical technique for characterizing membranes in research and production settings. It provides crucial insights into membrane materials' molecular structure and chemical composition, aiding in understanding their properties and behavior. FTIR analysis enables the determination of the chemical makeup

of membranes, including the types of polymers and additives utilized in their fabrication. Producers can assess membrane composition's homogeneity by comparing FTIR spectra across different batches or samples, ensuring production consistency and quality.

Moreover, FTIR is indispensable for identifying changes in membrane chemical structure resulting from chemical treatments or modifications. This capability is essential for evaluating the effects of such alterations on membrane properties. FTIR facilitates research into membrane interactions with other substances, such as contaminants or solvents, providing valuable insights into membrane suitability for specific environmental conditions. Detailed FTIR spectra offer information on molecular structure aspects such as polymer chain arrangement, crystallinity, and bond presence or absence.

Ultimately, the overarching objective of FTIR analysis in membrane studies is to attain a comprehensive understanding of the molecular structure and chemical composition. This knowledge is essential for quality control in production, assessment of modifications, and examination of membrane compatibility with diverse substances.

In this research, Fourier Transform Infrared Spectroscopy (FTIR) was employed to investigate the chemical properties of the membrane. A thin membrane sheet was used to measure within a designated sample container. FTIR spectra were obtained using the Nicolet iZ10 instrument from Thermo Scientific, USA, operating within the wavelength range of 4000 to 400  $\text{cm}^{-1}$ , facilitating gas analysis.

The FTIR analysis was employed to examine the chemical compositions of the PVDF membrane.

#### **4.7.2 SEM-EDS**

The research scrutinized the layers' surface features and chemical composition, employing a Zeiss Ultra Plus scanning electron microscope (SEM) outfitted with an Oxford X-Max 20 energy-dispersive (EDS) detector. Surface attributes were assessed at accelerating voltages (AVs) of 5 and 10 kV. EDS spectra were captured at 5 kV to accommodate potential particulate matter. Quantitative analysis was conducted utilizing peaks associated with carbon (C-K $\alpha$ ), fluorine (F-K $\alpha$ ), oxygen (O-K $\alpha$ ), silver (Ag-LI, Ag-L $\alpha$ ), copper (Cu-L $\alpha$ ), and titanium (Ti-K $\alpha$ , Ti-L $\alpha$ ). A single specimen of each membrane was utilized for both surface morphology and SEM-EDS examination.

#### **4.7.3 Contact Angle**

One method that is frequently used to evaluate the hydrophilicity of a membrane surface is contact angle measurement. The junction of the membrane surface and a tangent to the curved surface of a liquid droplet form this angle. An inverse link exists between the contact angle value and the membrane's wettability. Said another way, a smaller contact angle indicates more excellent membrane wettability. Put otherwise, the membrane exhibits an increasing affinity for water or other wetting liquids as the contact angle lowers, indicating a greater propensity to interact with and be wetted by the fluid. This relationship plays a critical role in comprehending the efficiency with which a membrane surface can enable interactions with liquids. It is essential in many applications, especially material science, filtration, and membrane technology [28,39]

The tangent angle at which a liquid drop forms on a solid surface is measured in contact angle measurements. When evaluating interfacial tensions between solid-vapor and solid-liquid phases, contact angles ( $\theta$ ) are helpful since they are easy to count on properly prepared solid surfaces [39].

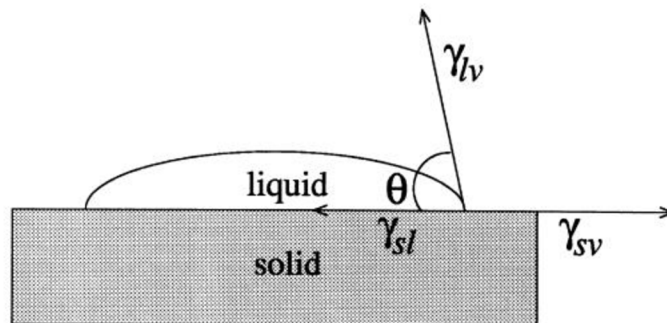
Young discovered a relationship that provides the basis for inferring solid surface tensions from contact angles. Through the interaction of three interfacial tensions—solid-vapor ( $\gamma$ ), solid-liquid ( $\gamma_u$ ), and liquid-vapor ( $\gamma$ )—you can get the contact angle of a liquid drop on a solid surface using Young's equation. Young's equation captures this condition of balance. Young extended the application of the equilibrium contact angle measurement to any liquid droplet by becoming the first to do it on a smooth, non-textured surface. The following **Eqn.3** provides an expression for this idea [39].

**Equation 3 Young's equation for contact angle**

$$\cos \theta = \frac{\gamma_{sv} - \gamma_{sl}}{\gamma_{lv}}$$

- The equilibrium contact angle, expressed in degrees, is denoted by the symbol  $\theta$ .
- The phases of a substance are denoted by the letters S, l, and v, respectively.
- The  $\gamma$  represents the interfacial tension, expressed in milli-Newtons per meter (MN/m). Here,  $\gamma_{sv}$ , known as solid surface energy, represents the interfacial tension between the solid and vapor phases. The interfacial tension between the solid and liquid phases is represented by  $\gamma_{sl}$ , whereas the liquid surface tension, or  $\gamma_{lv}$ , is the interfacial tension between the liquid and vapor phases.

The schematic of a contact angle system featuring a sessile-drop configuration is shown in **Figure 12**, where  $\theta_Y$  stands for Young's contact angle.



**Figure 12. Schematic of a contact angle system featuring a sessile-drop configuration [39]**

A surface's classification is based on a water droplet's contact angle (shown as  $\gamma$ ). When  $\gamma < 90^\circ$ , a surface is classified as super hydrophilic; when  $\gamma > 90^\circ$ , it is classified as hydrophilic; and when  $\gamma > 90^\circ$ , it is classified as hydrophobic. The highest contact angle measured for a water droplet on a smooth surface is about  $130^\circ$  [39,37].

A surface's wetting capacity can be categorized based on the contact angle value [37].

- Super hydrophilic when  $\theta \approx 0^\circ$ .

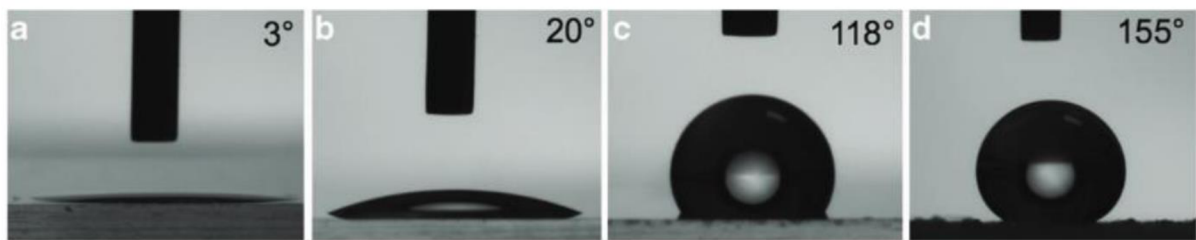
- Hydrophilic when  $\theta < 90^\circ$ .
- Hydrophobic when  $\theta > 90^\circ$ .
- Superhydrophobic when  $\theta > 150^\circ$  and the contact angle hysteresis is below  $5^\circ$ .

a) Super hydrophilic surface with  $\theta = 3^\circ$ . b) Hydrophilic surface with  $\theta = 20^\circ$

c) Hydrophobic surface with  $\theta = 118^\circ$

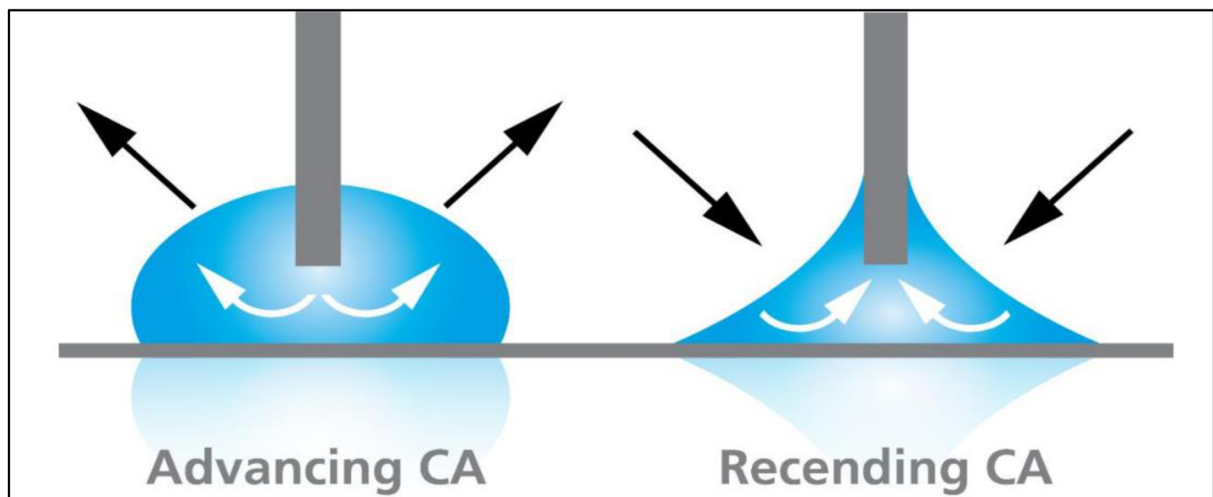
d) Superhydrophobic surface with  $\theta = 155^\circ$  and very low contact angle hysteresis

The contact angle between various surface substrates and water droplets is displayed in **Figure 13**.



**Figure 13. Classification of Surface wetting ability by contact angle.[37]**

The difference between the highest and minimum contact angles measured on a solid surface is called contact angle hysteresis. Surface heterogeneity and roughness are usually the source of this phenomenon. Physically speaking, contact angle hysteresis estimates the energy lost when a liquid droplet moves across a solid surface. The entire interfacial area between the liquid droplet and the concrete surface dramatically influences the contact angle hysteresis. More specifically, a decrease in contact angle hysteresis is correlated with a reduction in the solid-liquid interfacial area. **Figure 14** shows the advancing and receding contact angles [37].



**Figure 14. The advancing and the receding contact angle.[37]**

This research study used the sessile drop method to directly measure the membrane's water contact angle. This method clearly illustrates how well a membrane surface wets in response to the application of liquid [37].

A deionized water droplet was dispensed onto a dry membrane surface through a small tip to perform the measurement. Using the Drop Shape Analyzer DSA30E from KRÜSS GmbH as the liquid-dispensed Controller to see the droplet image and determine the water contact angle,

the DSA4 - Drop Shape Analysis software was used at room temperature. With the aid of the image analysis software, the final contact angle result was calculated as the average value of the right and left angles [37].

#### 4.7.4 Water uptake and swelling of the membrane

The membrane's porosity, reflecting its hydrophilicity and hydrophobicity, is predominantly assessed through water absorption. The disparity between the dry membrane's weight and the fully immersed membrane indicates its water absorption capacity [40,48].

Water absorption, pivotal in filtering technology, is closely intertwined with membrane porosity and dictates its hydrophilic properties. The membrane's capacity to adsorb water underscores its water absorption, a critical attribute in filtration mechanisms [48].

Moreover, the swelling degree is a gauge of membrane performance, determined by immersing the membrane in deionized water and comparing its dimensions to its dried state. A lower swelling ratio suggests enhanced membrane stability due to stiffer voids within the membrane matrix. This stability is inversely correlated with the swelling degree; lower swelling denotes heightened membrane stability [40,48].

The experimental procedure involves initially recording the weight and dimensions of dehydrated membranes, followed by a 24-hour drying period at room temperature. Subsequently, the dried membranes were fully submerged in deionized water for 24 hours to attain saturation. Following this procedure, the hydrated membranes were removed from the water, excess water was promptly removed using absorbent paper, and the dimensions and weight of the hydrated forms were documented. The specimen's area is utilized to calculate water uptake and swelling degree, employing specific formulas outlined in **Eqn 4**. shows And **Eqn. 5** below.

##### *Equation 4 Formula for water uptake calculation*

$$WU (\%) = \frac{W_{wet} - W_{dry}}{W_{dry}} \times 100\%$$

- WU (unit in %) denoted for the water uptake value.

-  $W_{wet}$ ,  $W_{dry}$  (unit in gram or milligram) denoted for the weight of wet and dry membrane samples, respectively.

##### *Equation 5 Formula for swelling degree calculation*

$$SD (\%) = \frac{a_{wet} - a_{dry}}{a_{dry}} \times 100\%$$

- SD (unit in percentage) denoted for the swelling degree value,

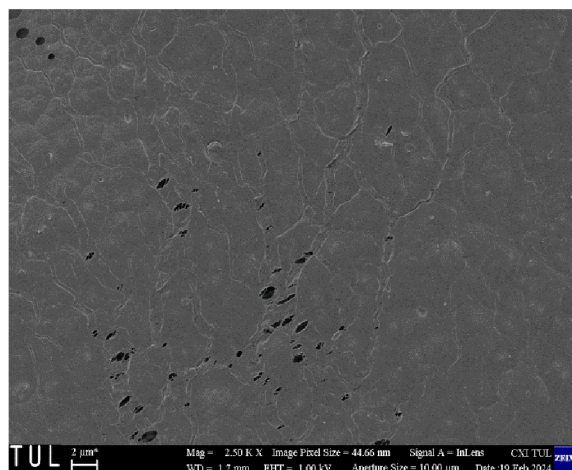
-  $a_{wet}$ ,  $a_{dry}$  (unit in squared centimetres) denoted for the area of hydrated and dry membrane samples, respectively.

## 5. Result & Discussion

### 5.1 Membrane Characterization

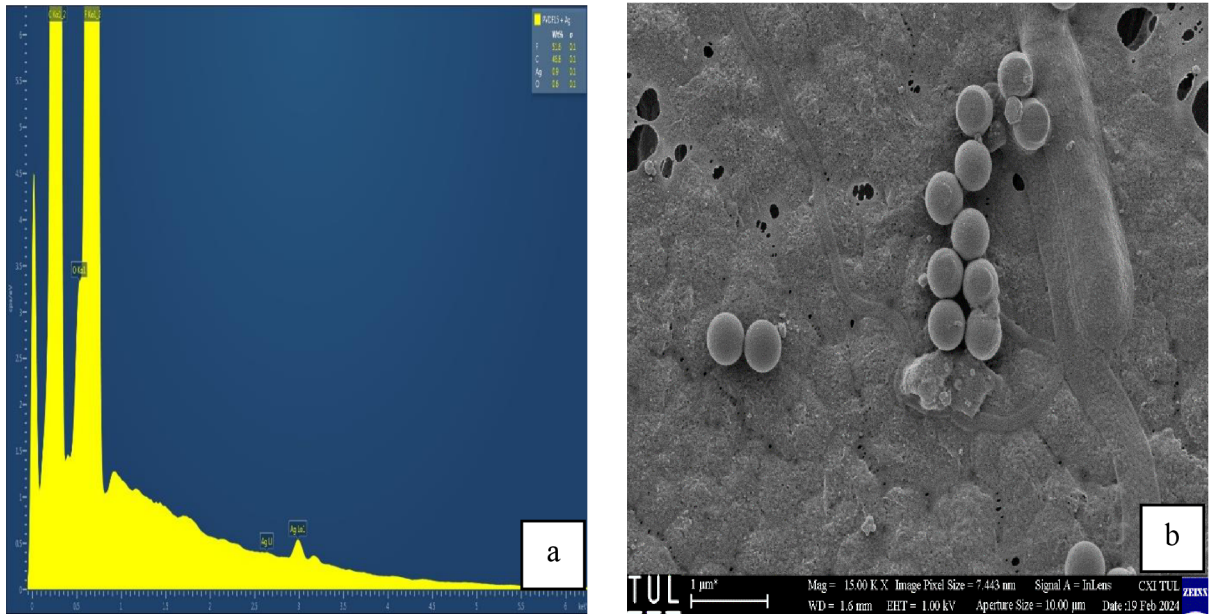
#### 5.1.1 Membrane Morphology of PVDF 15% wt. and PVDF 20% wt by SEM-EDS

SEM-EDS spectra were analysed to ascertain the presence of nanoparticles on the membrane surface. Each graph depicting the spectra from individual membranes reveals conclusive evidence of nanoparticle and microparticle presence on the membrane surface. SEM images show the surface morphology analyses of all membranes.



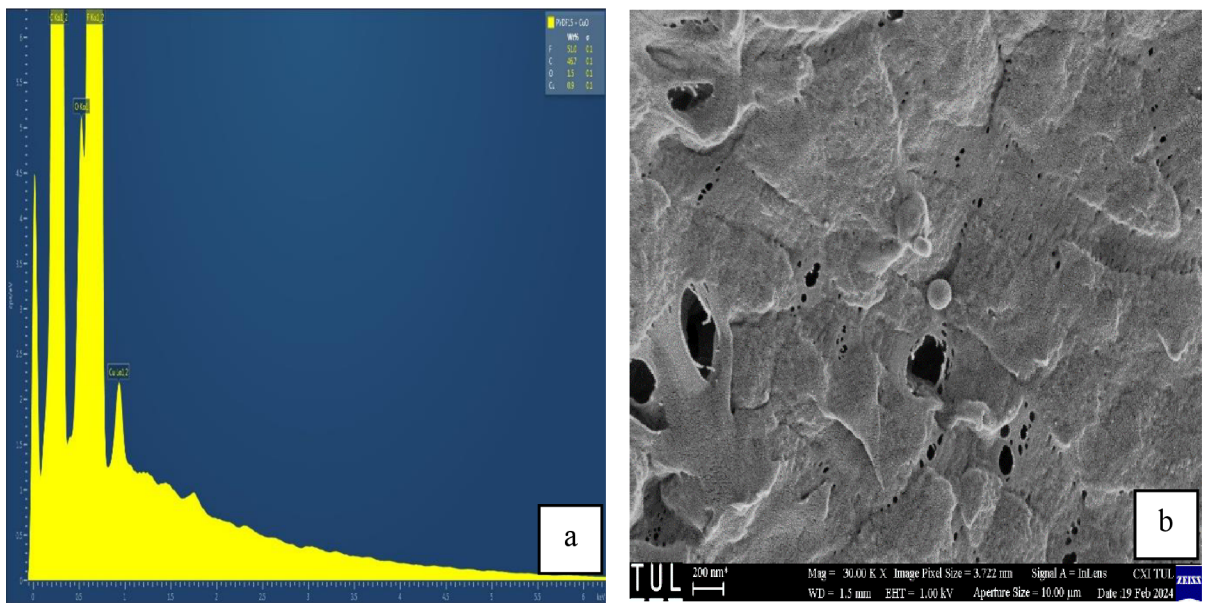
*Figure 15 Surface morphology of PVDF15% wt.*

**Figures 15** illustrate the surface morphology of membrane fabricated with PVDF15% wt membrane exhibits a smoother surface than the modified membranes, indicating the absence of nanoparticles or microparticles.



**Figure 16. a) EDS spectrum of PVDF15% wt AgNO<sub>3</sub>, b) surface morphology of PVDF15% wt AgNO<sub>3</sub> by SEM.**

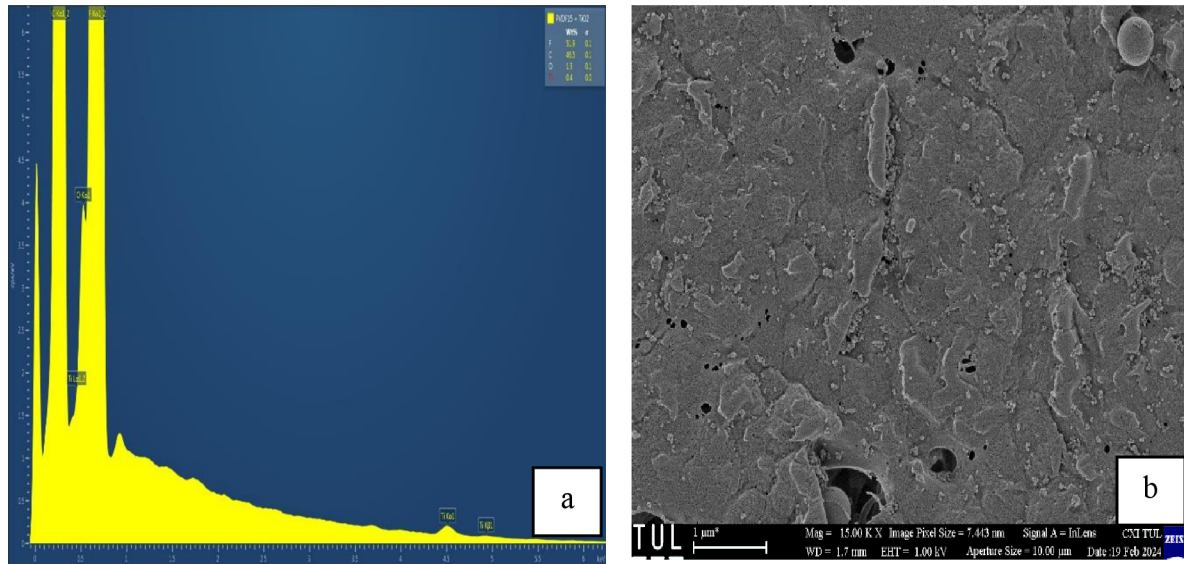
**Figure 16 (a and b)** indicates the SEM-EDS analysis of PVDF15% AgNO<sub>3</sub>. The presence of Ag nanoparticles is visible in EDS spectrum **Figure 16(a)**. The EDS pattern indicates that 0.9 % wt. presence of Ag metal. This proves that nanoparticles exist in the modified membrane, **Figure 16 (b)**. The modified membrane changed the surface roughness, with visible nanoparticles. In particular, **Figure 16 (b)** depicts the accumulation of AgNO<sub>3</sub> nanoparticles and EDS spectrum confirms the presence of AgNO<sub>3</sub> nanoparticles.



**Figure 17. a) EDS spectrum of PVDF15% wt CuO, b) surface morphology of PVDF15% wt CuO by SEM.**

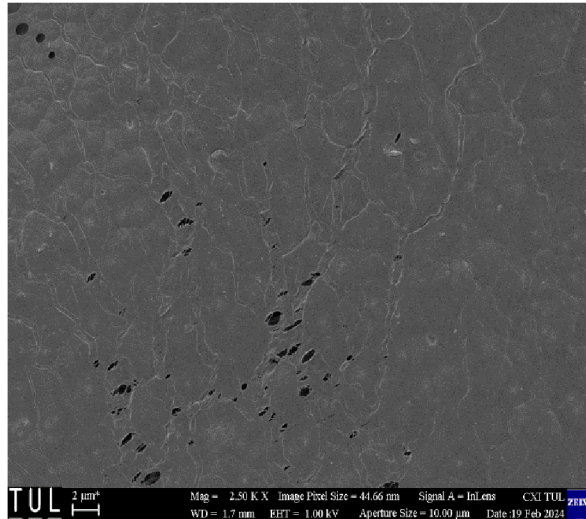


In **Figure 17(a)**, the EDS spectrum reveals the detection of microparticles containing CuO, constituting 0.9% wt. This observation suggests the influence of CuO microparticles on the membrane surface, as further evidenced by SEM imaging. In **Figure 17(b)**, the SEM image illustrates alterations in the surface morphology of the membrane attributable to the presence of CuO microparticles. The microparticle is evenly spread on the surface, indicating effective modification.



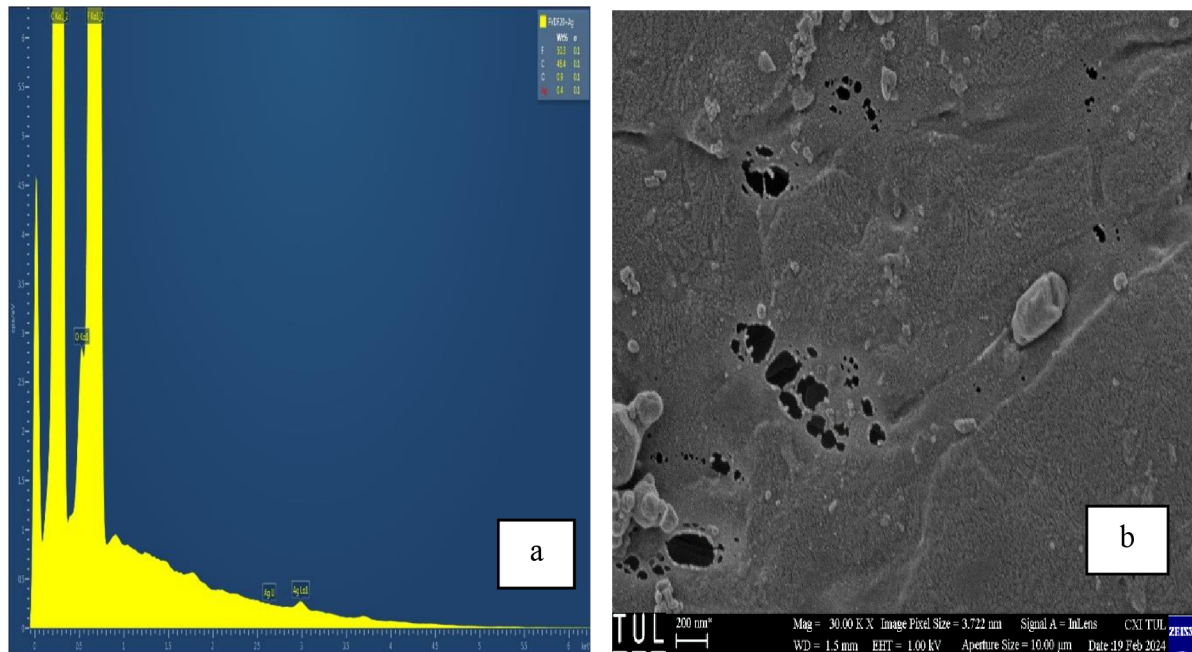
**Figure 18. a) EDS spectrum of PVDF 15% wt TiO<sub>2</sub>, b) surface morphology of PVDF 15% wt TiO<sub>2</sub> by SEM.**

The EDS spectrum of PVDF 15% wt TiO<sub>2</sub> is shown in Figure 18(a), where Ti particles account for 0.4% wt. SEM analysis, which is shown in **Figure 18(b)**, verifies that TiO<sub>2</sub> nanoparticles are present on the membrane surface. Interestingly, these nanoparticles have are easily observed on their surface.



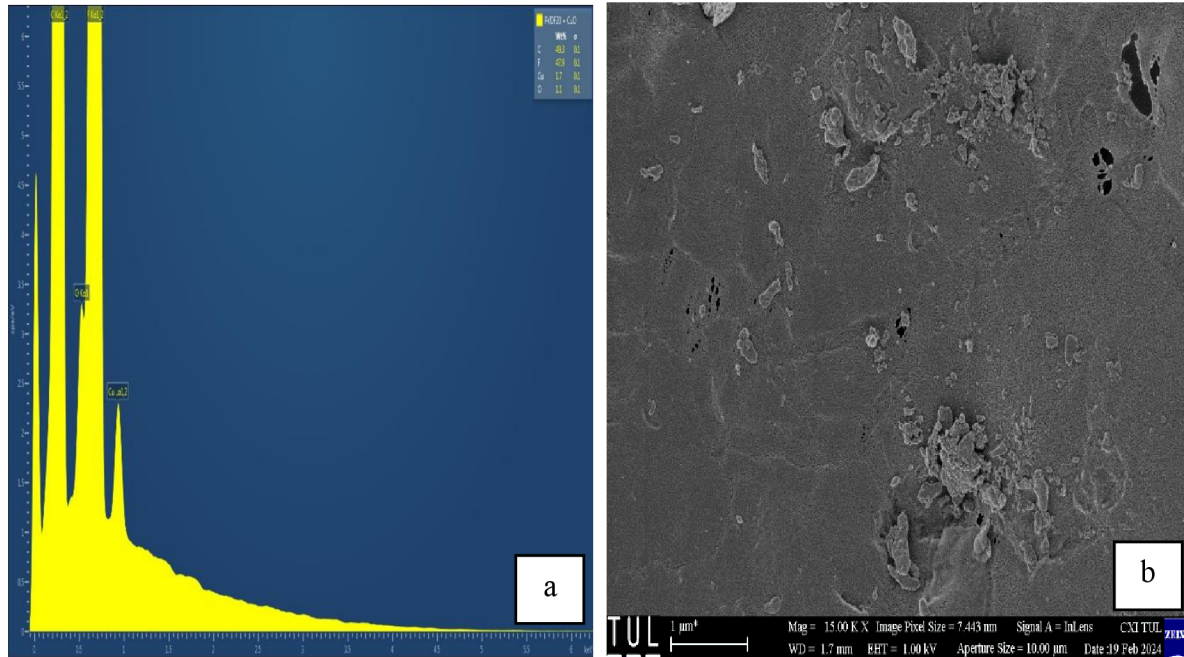
**Figure 19** Surface morphology of PVDF 20%

**Figure 19** shows that the surface morphology analysis of membranes fabricated using PVDF 20%wt reveals a distinctly smoother surface texture than the modified membranes. This smoother surface appearance suggests an absence of nanoparticles and microparticles on the membrane surface. This observation underscores the potential influence of the modification process on the surface characteristics of the membranes, indicating a clear distinction in surface morphology between the unmodified and modified membrane samples.



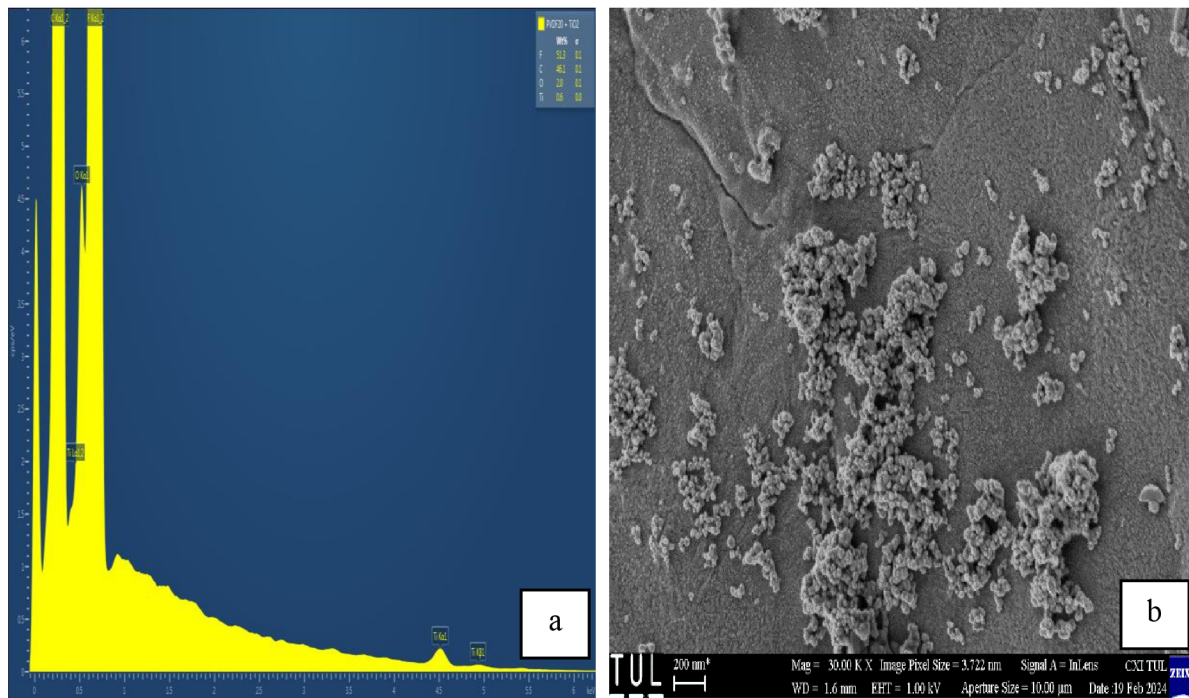
**Figure 20.** a) EDS spectrum of PVDF 20% AgNO<sub>3</sub>, b) surface morphology of PVDF 20% AgNO<sub>3</sub> by SEM

**Figure 20 a)** EDS spectra illustrates the PVDF 20% AgNO<sub>3</sub>. There are visible Ag nanoparticles. The EDS pattern shows that the presence of Ag metal is 0.4% wt. Proof that there are nanoparticles in the modified membrane, **Figure 20 b)** SEM image of PVDF 20% exhibit particle agglomeration bonds, indicating surface modification and Ag seem to get more firmly attached to the membrane's surface, clearly shows the difference on membrane surface.



**Figure 21. a)** EDS spectrum of PVDF 20% CuO, **b)** surface morphology of PVDF 20% CuO by SEM

**Figure 21 a)** shows the CuO microparticle present on membrane surface, the result shows the presence of Cu is 1.7 % wt, it is the highest of all other membranes, **Figure 21 b)** SEM analysis shows the rough surface and CuO microparticles are visible on surface.



**Figure 22. EDS spectrum of PVDF 20% TiO<sub>2</sub> b) surface morphology of PVDF 20% TiO<sub>2</sub> by SEM.**

The EDS spectrum of PVDF 20% wt TiO<sub>2</sub> is shown in **Figure 22(a)**, where TiO<sub>2</sub> particles account for 0.6% wt. SEM analysis, which is shown in **Figure 22(b)**, verifies that TiO<sub>2</sub> nanoparticles are present on the membrane surface. Interestingly, these nanoparticles are easily observed on their surface

These nanoparticles and microparticle modifications are expected to enhance the membrane hydrophilicity and antifouling performance by enhancing the hydrophilic functional groups on the membrane surface. Moreover, using alkaline treatment causes defluorinating the fluorine group present in PVDF, which is exchanged F with hydroxyl (-OH) hydrophilic functional group [38,42,43,44]. To prove it FTIR test has been done and results shown in section 5.3.

## 5.2 Pore Size

*Table 4 pore size measurement of PVDF 15% wt.*

Sample no.	Sample Name	Average Surface Pore Size (in Nm)
1	PVDF 15%	618.77±142.87
2	PVDF 15% Tio2	535.13±160.78
3	PVDF 15% Agno3	425.61±63.71
4	PVDF 15% CUO	179.24±65.91

*Table 5 Pore size of PVDF 20% wt.*

Sample no.	Sample Name	Average Surface Pore Size (in Nm)
1	PVDF 20%	527.85±191.67
2	PVDF 20% CUO	349.57±120.58
3	PVDF 20% Agno3	516.01±117.92
4	PVDF 20% Tio2	UNDEFINED

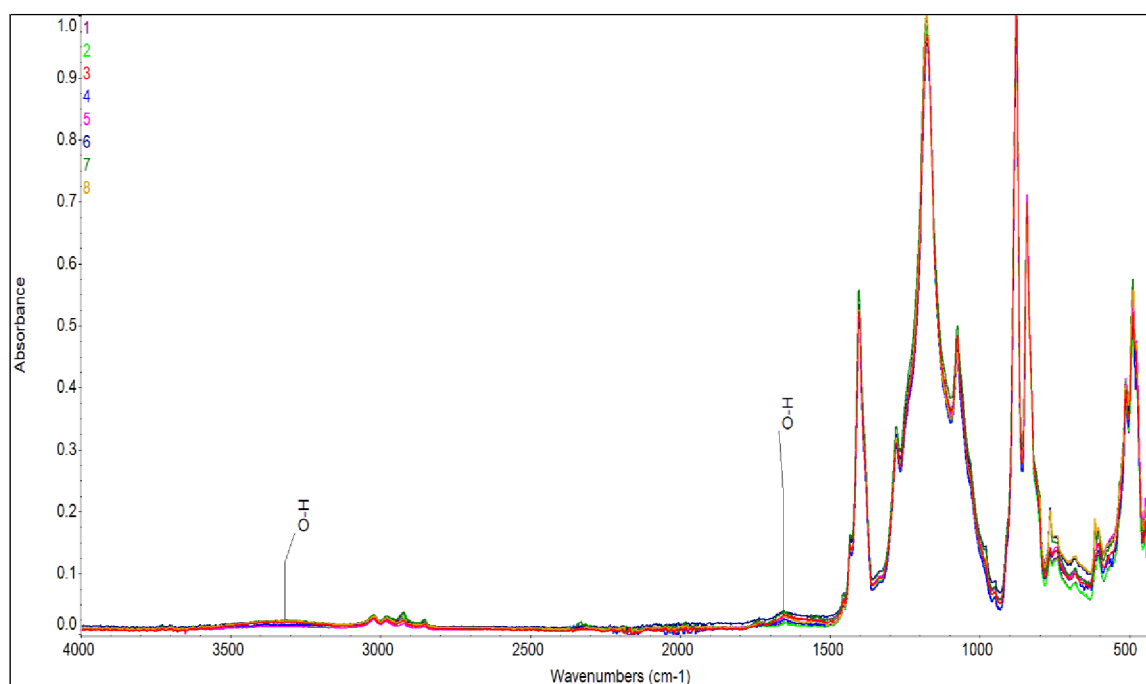
The Pore size measurement was conducted using ImageJ software, it is seen from **Table 4** revealed that the average pore size of pristine PVDF 15% wt. Membranes is 618.77±142.87, while **Table 5** for PVDF 20% wt. Membranes, it is 527.85±191.67. This observed variation may be attributed to the higher concentration and viscosity of the PVDF 20% wt compared to PVDF 15% wt.

Increasing the viscosity of the polymeric solution tends to prolong the formation of microvoids during the Non-Solvent-Induced Phase Separation (NIPS) process. However, it concurrently

enhances the interconnectivity within the pore matrix. This is achieved by impeding the exchange of solvent and nonsolvent during the NIPS process [37].

Simultaneously, a smaller pore size on the top dense skin layer during membrane creation may result from a more complicated porous sublayer [31]. Table 4 shows that after surface modification treatment with alkali nanoparticle/microparticle, PVDF15% wt. The modified membrane's average pore size has been reduced. It is believed that pore size has decreased due to pore swelling after alkali and particle treatment [30]. As seen in **Table 5**, PVDF 20% wt. Tio<sub>2</sub>, it was impossible to measure the pore size via the image J program due to pore shrinkage after surface modification; as we can see, nanoparticle adhesion on the surface pores is extremely small.

### 5.3 FTIR



**Figure 23 FTIR Spectra of PVDF Membranes before and after surface modification**

**(1-PVDF15% wt, 2- PVDF20% wt, 3- PVDF20% wt AgNO<sub>3</sub>, 4- PVDF20% wt TiO<sub>2</sub>, 5- PVDF20% wt CuO, 6- PVDF15% wt AgNO<sub>3</sub>, 7- PVDF15% wt CuO, 8—PVDF15% wt TiO<sub>2</sub>)**

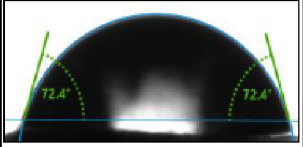
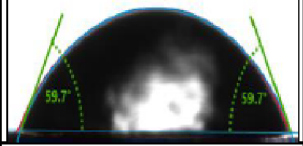


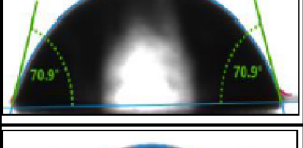

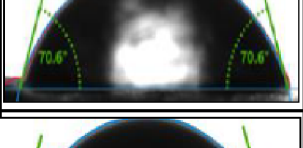

FTIR spectroscopy was employed to validate the presence of hydroxyl (OH) groups in the membrane after surface modification. The treatment of PVDF involves oxidative reactions and dehydrochlorination of fluorine groups, particularly after alkaline treatment and nanoparticle surface modification. This chemical transformation leads to the emergence of hydroxyl groups on the membrane's surface, thus imbuing it with hydrophilic properties and enhancing its antifouling performance [30].

The FTIR spectra in **Figure 23** exhibit two notable additional peaks. The first peak, centered at 3350 cm<sup>-1</sup>, appears to overshadow the peaks associated with CH<sub>2</sub> stretching vibrations. The second peak, at 1650 cm<sup>-1</sup>, signifies the presence of hydroxyl -OH groups on the PVDF membrane surface post-alkaline treatment, denoted as PVDF-OH groups.

The peak detection at 1650 cm<sup>-1</sup> underscores the incorporation of hydroxyl -OH groups onto the membrane's surface. This signifies the successful modification of the polymer surface, resulting in the introduction of hydroxyl functional groups. These findings offer valuable insights into the structural alterations occurring during the dehydrochlorination process of PVDF [30].

## 5.4 Contact Angle

*Table 6 Contact Angle data with images*

Sample No	Sample Abbrivation	Contact angle Value(°)			Image
		L Side	R side	Average	
1	PVDF-20	72.05	72.05	72.05	
2	PVDF-20 AgNO3	59.86	59.86	59.86	
3	PVDF-20 CuO	62.75	62.61	62.68	
4	PVDF-20 TiO2	59.23	57.52	58.375	
5	PVDF-15	71.01	71.01	71.01	
6	PVDF-15 AgNO3	67.5	67.5	67.5	
7	PVDF-15 CuO	70.6	70.6	70.6	
8	PVDF-15 TiO2	63.96	64.26	64.11	

Contact angle measurement is a widely accepted technique for evaluating the hydrophilicity of membrane surfaces [26]. In this study, contact angle measurements were performed on pristine PVDF20% wt and PVDF15% wt concentrations, resulting in angles of 72.05° and 71.01°, respectively. It should be noted that contact angle values are influenced by pore size, surface morphology, roughness, and pore diameter. The contact angle values obtained, all below 90° as presented in **Table 6**, suggest the hydrophilic nature of the membranes, which is advantageous for filtration applications.



Despite its common usage in membrane casting, PVDF exhibits inherent hydrophobicity, necessitating surface modification to enhance hydrophilicity and facilitate nanoparticle and microparticle adhesion. Alkali treatment is employed for such modification, enabling the integration of nanoparticles and surface hydrophilization [27]. The contact angle measurements detailed in **Table 6** underscore the efficacy of this modification process. Notably, contact angles for PVDF 20% wt membranes modified with nanoparticle AgNO<sub>3</sub>, TiO<sub>2</sub>, and microparticle CuO weight concentration demonstrate significant reductions at 59.86°, 58.37°, and 62.68°, respectively. The results prove that after indicative modification with alkali and micro- and nano-particles had more hydrophilic functional groups and changed the membrane's hydrophilicity [27].

As seen from **Table 6**, the contact angle of pristine PVDF 15% wt and modified PVDF 15% wt membranes has higher contact angle, which is possibly believed that increasing the concentration of PVDF solution impacted surface properties, which made the membrane more hydrophilic.[28]. It is possible that larger pore size and surface roughness caused the higher contact angle in PVDF 15% wt membranes. So it is assumed that PVDF 20% wt membrane has less rough surface and pore sizes than PVDF 15% wt [29].

## 5.5. Swelling test

*Table 7 Water Uptake data in %*

Sample Abbreviation	Weight in dry form (in grams)	Weight in wet form (in grams)	Water uptake (In percentage %)
PVDF 15%	0.0262	0.0267	1.9084
PVDF 15% Agno3	0.0271	0.0275	1.4760
PVDF 15% Cuo	0.0269	0.0273	1.4870
PVDF 15% Tio2	0.0266	0.0271	1.8797
PVDF 20%	0.0367	0.0379	3.2698
PVDF 20%	0.0376	0.0384	2.1277
PVDF 20%	0.0374	0.0379	1.3369
PVDF 20%	0.0379	0.0384	1.3193

*Table 8 Swelling Degree In percentage %*

Sample Abbreviation	Area in dry form (Cm <sup>2</sup> )	Area in wet form (Cm <sup>2</sup> )	Swelling degree (In percentage %)
PVDF 15%	7	7.6678	9.5400
PVDF 15% Agno3	7	7.9756	13.9371
PVDF 15% Cuo	7	7.9687	13.8386
PVDF 15% Tio2	7	7.9898	14.1400
PVDF 20%	7	7.9065	12.9500
PVDF 20%	7	7.9067	12.9529
PVDF 20%	7	7.9046	12.9229
PVDF 20%	7	7.9049	12.9271

**Table 7** and **Table 8** present the water uptake percentage and swelling degree percentage, respectively, indicating the membrane's response to immersion in water. As seen in **Table 7**, it did not show any notable changes. On the other side, the swelling test, as seen in **Table 8**, showed membrane dimensions changed slightly. PVDF 15% wt. showed different dimensional changes after modification compared to pristine ones. The reason could be due to low

concentration and less compact membrane structure and highly hydrophilic groups on the membrane cause water absorption and membrane swelling. PVDF 20% wt showed the same swelling percentage before and after modification. The dense structure of PVDF 20% wt. does not allow the membrane swelling. The membranes have maintained their stability after being submerged in water. The lack of significant changes in these parameters post-immersion suggests that the membrane retains its structural integrity and stability in aqueous environments [40,29].

## 5.6. Permeability and Rejection

**Error! Reference source not found.** to **Error! Reference source not found.** depict the permeability and rejection performance of selected membranes. The filtration test comprised three separate runs for each sample, with three samples from each membrane being tested. During each run, 40 ml of microplastic-contaminated water was filtered through the membrane. Following each filtration run, the membrane underwent a rudimentary washing procedure with distilled water. The illustrated graphs provide a visual representation of the test results.

The investigation reveals that surface modification contributes to increased membrane permeability, consistent with findings from contact angle measurements, which demonstrated decreased contact angles after nanoparticle integration onto the membrane surface. Notably, the highest contact angles were observed for pristine PVDF 15% wt. Membranes and PVDF 20% wt. Membrane indicating membrane surface morphology's influence on permeability and rejection properties.

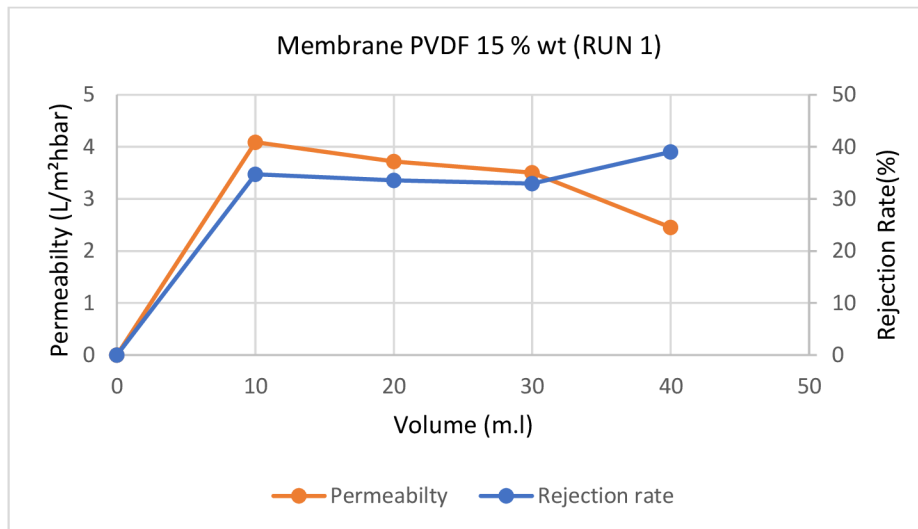
Furthermore, membrane permeability and rejection rates are contingent upon the density of membrane pore size, with higher PVDF concentrations yielding denser membranes. This study demonstrates that elevated PVDF concentration correlates with enhanced rejection rates, rendering them more effective for microplastic removal from contaminated water sources.

Moreover, surface modification amplifies membrane permeability and rejection rates by activating OH groups within the membrane, thereby rendering it more porous and hydrophilic. However, it is observed that pristine PVDF membranes at 15% and 20% weight concentrations are prone to membrane fouling, a phenomenon exacerbated by surface modification with nanoparticles. As depicted in **Figure 24**, pristine PVDF 15% wt membrane permeability and rejection rate went to, and permeability decreased to 2.45 L/m<sup>2</sup>h bar by 40. ml. After 1<sup>st</sup> run, only Membrane was blocked and wasn't working for another run. Almost similar phenomena occur for pristine PVDF 20% wt, which is illustrated in **Figure 34**

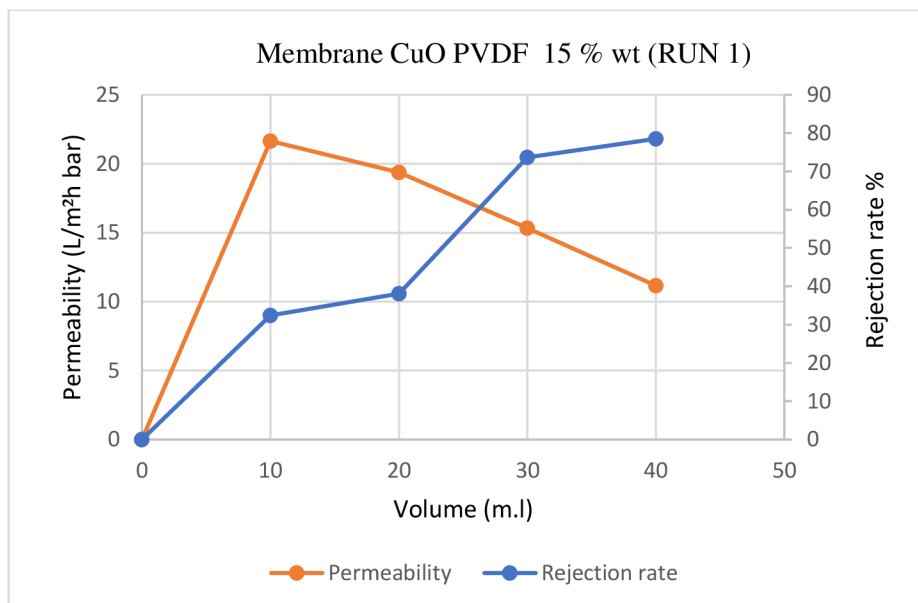
For instance, in **Figure 25**, **Figure 26**, and **Figure 27** portraying PVDF 15% CuO runs 1, 2, and 3, respectively, permeability initially rises to 21.65(L/m<sup>2</sup>h bar) in the first run for 10 ml., subsequently declining to 7.18 (L/m<sup>2</sup>h bar) by the third run for 40 ml., accompanied by an 85% increase in rejection rate. Similarly, in **Figure 28**, **Figure 29**, and **Figure 30** depicting PVDF 15% AgNO<sub>3</sub>, permeability peaks at 7.22(L/m<sup>2</sup>h bar) for 10 mL in the first run before dropping to 3.07 by the third run for 40 ml., with microplastic rejection rates reaching 99%.

In contrast, **Figure 31**, **Figure 32**, and **Figure 33** illustrate PVDF 15% TiO<sub>2</sub>, which indicates more stable permeability and 100% rejection rates during all three runs. Notably, the TiO<sub>2</sub> nanoparticle-modified membrane exhibits superior rejection rates and filtration performance compared to AgNO<sub>3</sub> and CuO counterparts. This observation aligns with contact angle results, where TiO<sub>2</sub> exhibited lower contact angles than AgNO<sub>3</sub> and CuO-modified membranes,

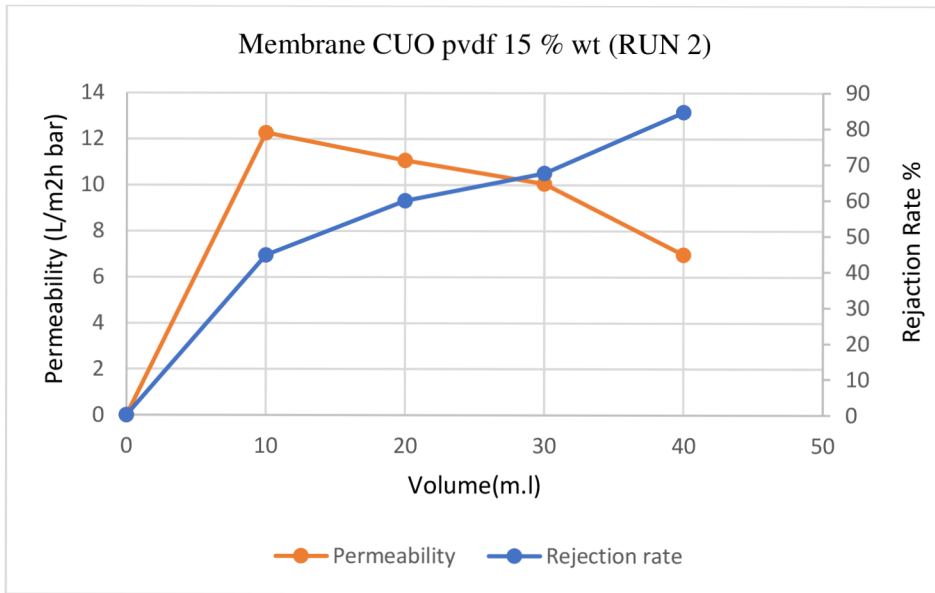
underscoring the direct relationship between permeability and surface morphology, pore size, and surface roughness. The permeability of PVDF increased by 15% after dehydrochlorination treatment and surface modification with nanoparticles and microparticles. Subsequently, it improved the rejection rate of microplastic.



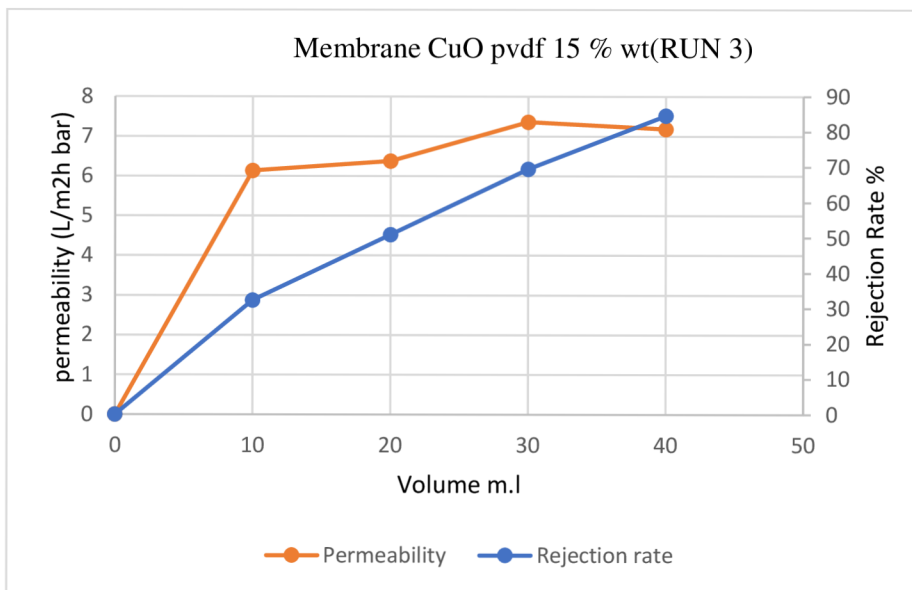
**Figure 24 Permeability and rejection of PVDF 15% wt**



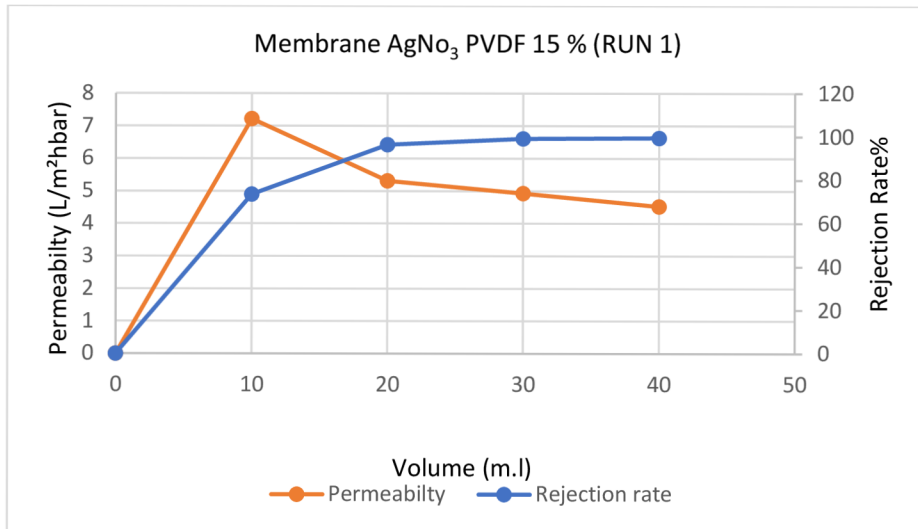
**Figure 25 Permeability and rejection of PVDF 15% CuO (run1)**



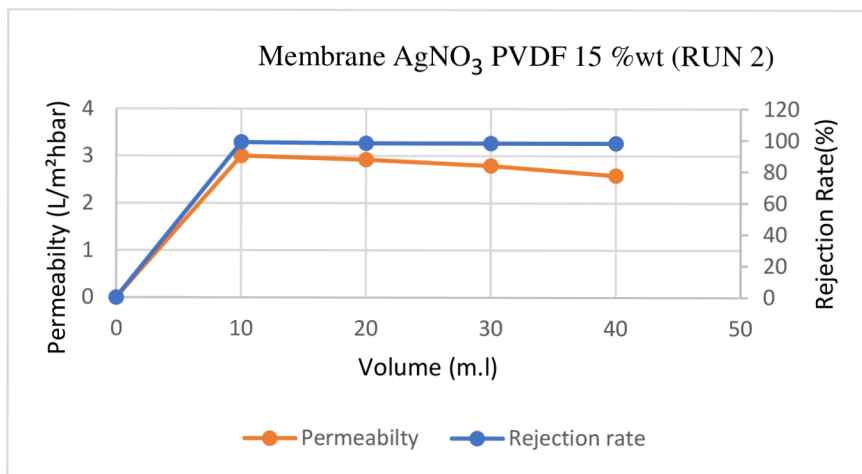
**Figure 26 Permeability and rejection of PVDF 15% CuO (run2)**



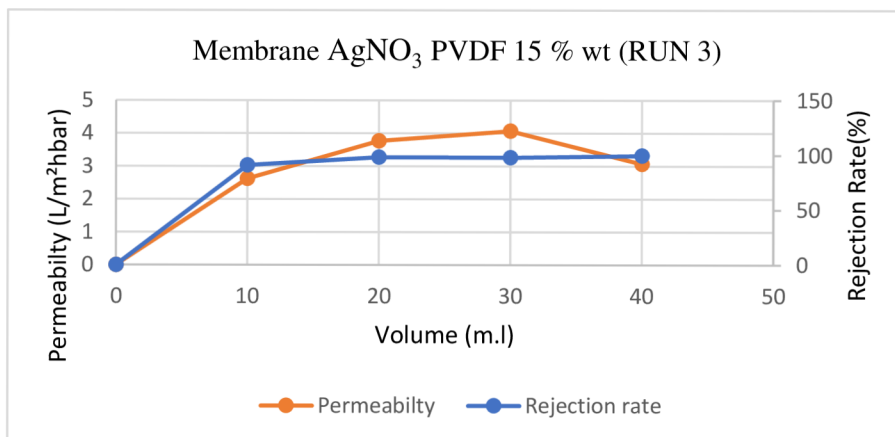
**Figure 27. Permeability, rejection, and antifouling of PVDF 15% CuO (run3)**



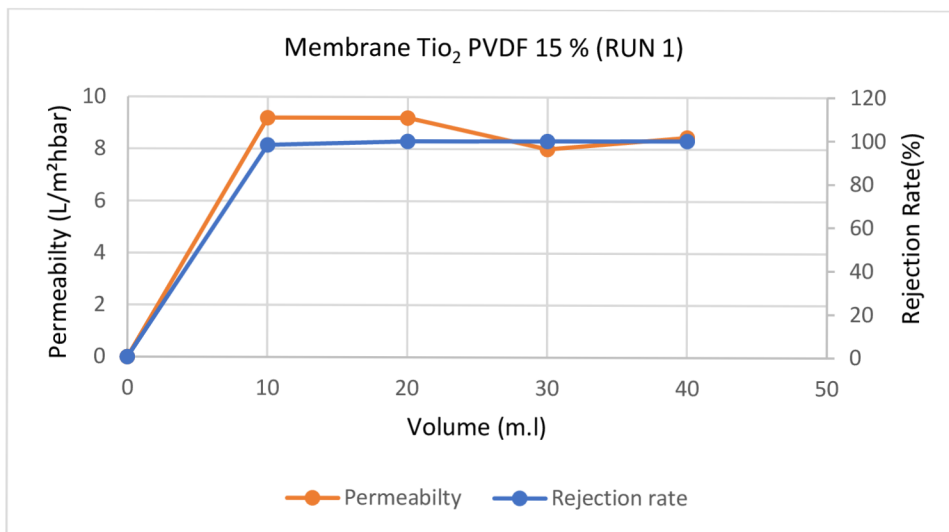
**Figure 28 Permeability and rejection of PVDF 15% AgNO<sub>3</sub> (run1)**



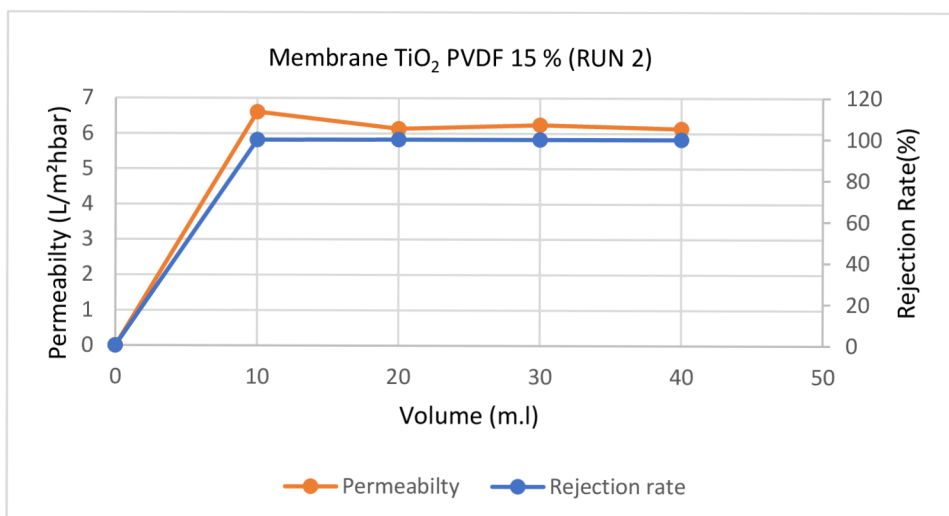
**Figure 29 Permeability and rejection of PVDF 15% wt AgNO<sub>3</sub> (run2)**



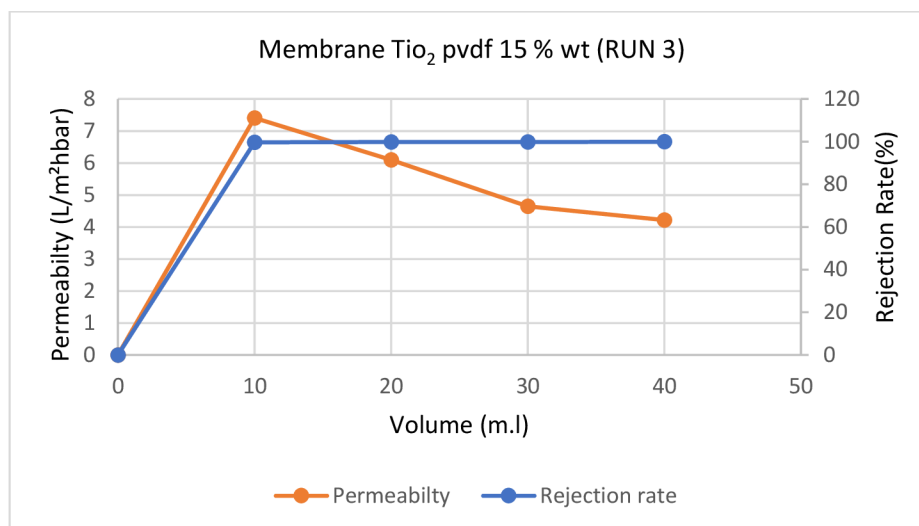
**Figure 30 Permeability and rejection of PVDF 15% wt AgNO<sub>3</sub>, (run3)**



**Figure 31 Permeability and rejection of PVDF 15% wt TiO<sub>2</sub> (run1)**



**Figure 32 Permeability and rejection of PVDF 15% wt. TiO<sub>2</sub> (run2)**



**Figure 33 Permeability, rejection, and antifouling of PVDF 15% wt. TiO<sub>2</sub> (run3)**

The performance of three different membrane types, PVDF 20% wt CuO, PVDF 20% wt AgNO<sub>3</sub>, and PVDF 20% wt TiO<sub>2</sub>, was evaluated regarding permeability and rejection rates during microplastic rejection experiments.

For the PVDF 20% wt CuO membrane, the initial permeability was 6.28 (L/m<sup>2</sup>h bar) with a rejection rate of 99%, represented in **Figure 35**. Subsequent runs demonstrated a gradual decline in permeability, reaching 3.41 (L/m<sup>2</sup>h bar) in the second run, shown in **Figure 36**, and further decreasing to 2.45 (L/m<sup>2</sup>h bar) in the third run, shown in **Figure 37**. Despite the decrease in permeability, the rejection rate remained 99% throughout all runs.

In contrast, the PVDF 20% wt AgNO<sub>3</sub> membrane depicted in **Figure 38** exhibited an initial permeability of 5.32 (L/m<sup>2</sup>h bar) with a rejection rate of 98%. Across subsequent runs, the permeability decreased to 3.51 (L/m<sup>2</sup>h bar) in the second run, Shown in **Figure 39**, and 2.73 (L/m<sup>2</sup>h bar) in the third run, represented in **Figure 40**. Notably, the rejection rate increased from 98% (figure 40) to 99% in the second run and maintained stability at 99% (figure 41) in the third run.

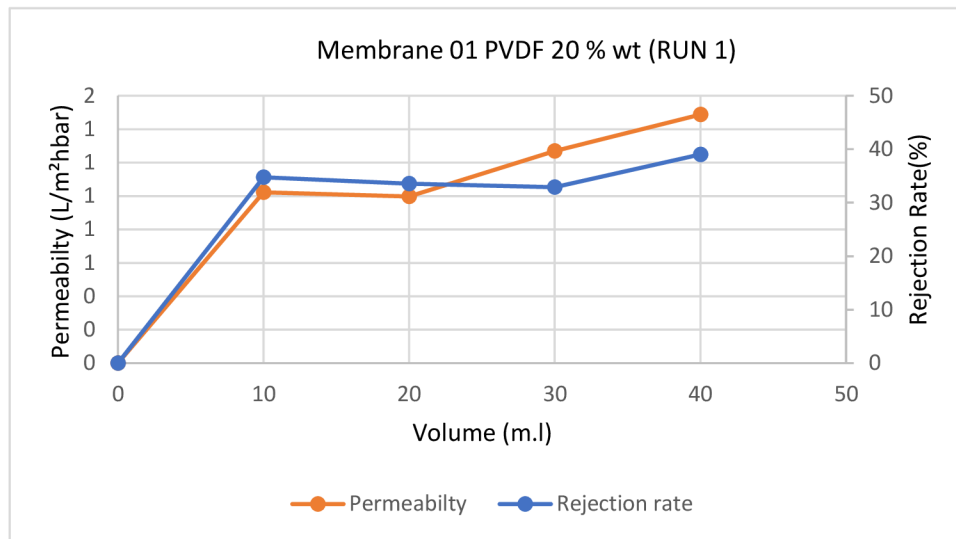
Finally, the PVDF 20% wt TiO<sub>2</sub> membrane depicted in **Figure 41** displayed an initial permeability of 2.89 (L/m<sup>2</sup>h bar) with a rejection rate of 99%. Subsequent runs resulted in a gradual decline in permeability to 2.67 (L/m<sup>2</sup>h bar), shown in **Figure 42** in the second run, and 2.23 (L/m<sup>2</sup>h bar) in the third run, shown In **Figure 43**. Interestingly, the rejection rate increased to 100% in the third run.

All three membrane types exhibited a decline in permeability across successive runs, indicating potential fouling or pore blockage. However, variations were observed in the behavior of rejection rates, with the PVDF 20% wt CuO and PVDF 20% wt AgNO<sub>3</sub> membranes maintaining stable rejection rates. In contrast, the PVDF 20% wt TiO<sub>2</sub> membrane achieved a 99% rejection rate in the third run. These results suggest distinct performance characteristics and potential applications for each membrane type in microplastic rejection processes.

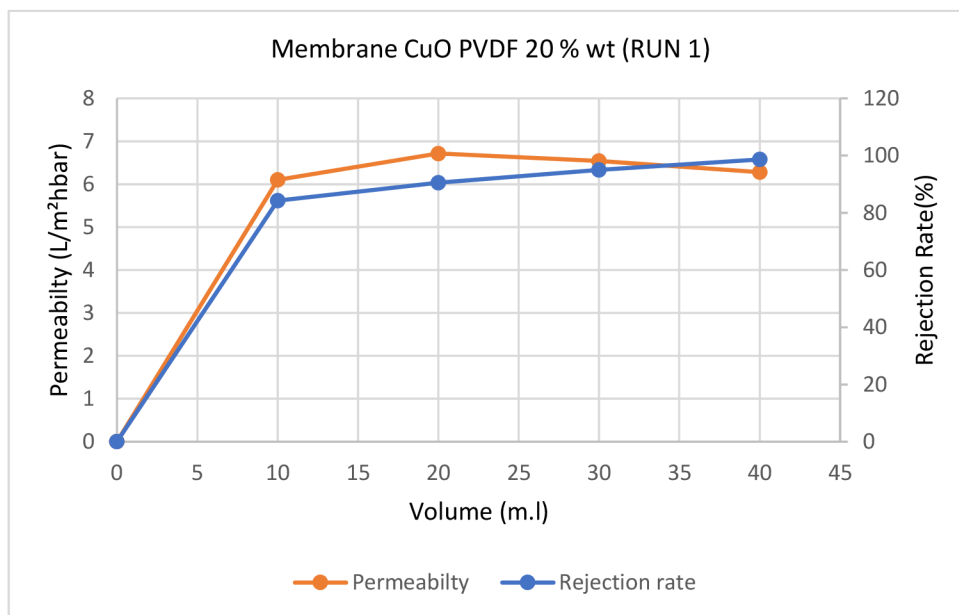
While both modified PVDF membranes exhibit a decline in permeability over successive runs, the PVDF 15% wt membrane demonstrates slightly higher initial permeability than the PVDF 20% wt membrane. Additionally, the TiO<sub>2</sub> modified PVDF 15% wt membrane consistently



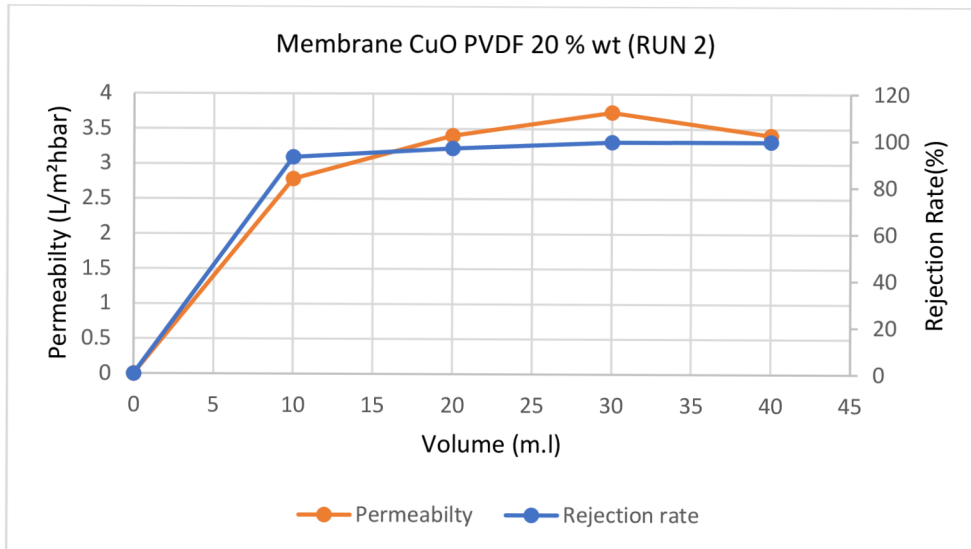
outperforms its PVDF 20% wt counterpart regarding rejection rates, suggesting potential advantages for TiO<sub>2</sub> surface modification in microplastic rejection applications.



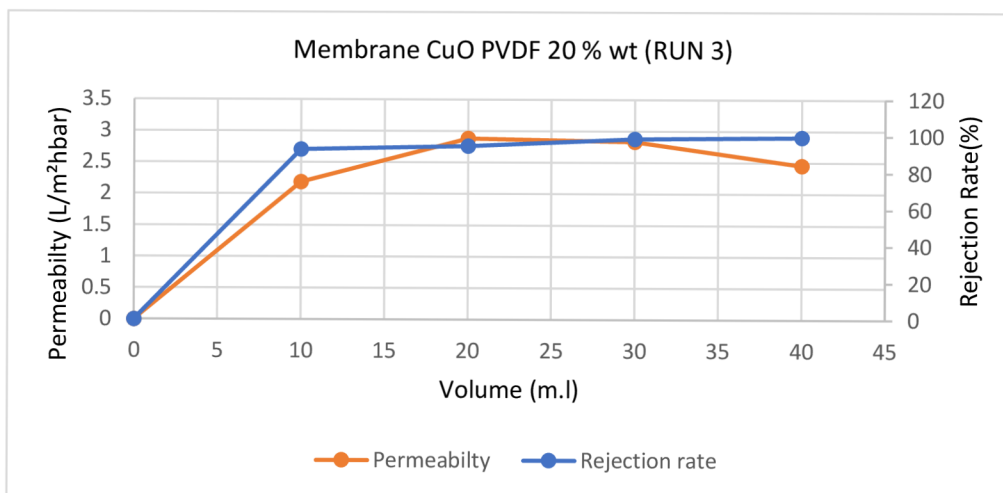
**Figure 34 permeability, rejection, of PVDF 20% wt.**



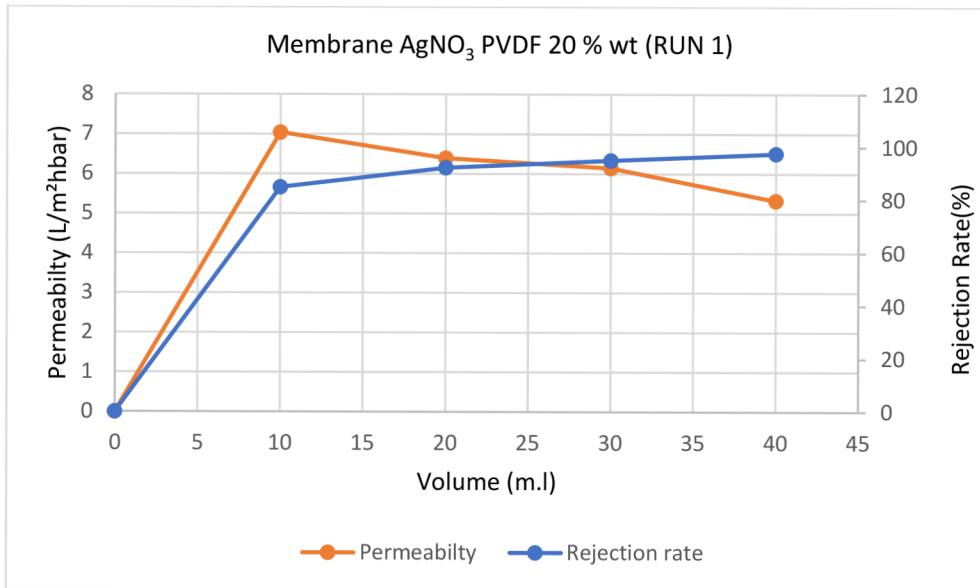
**Figure 35 Permeability and rejection of PVDF 20% wt CuO (run1)**



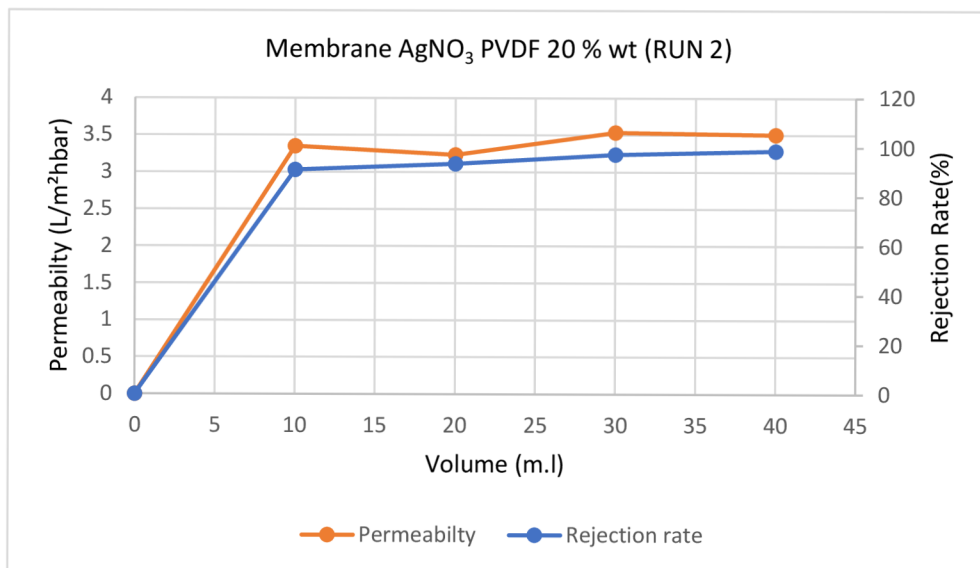
**Figure 36 Permeability and rejection of PVDF 20% wt CuO (run2)**



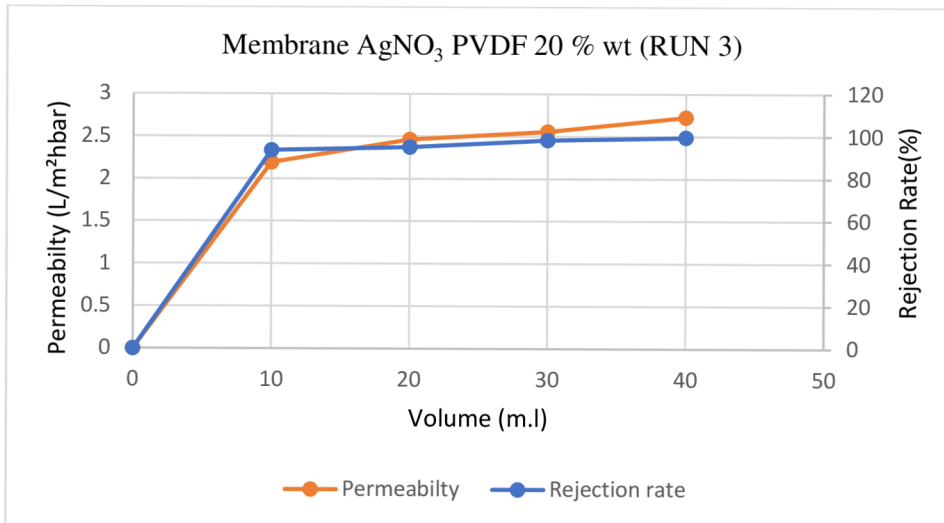
**Figure 37 Permeability and rejection of PVDF 20% wt CuO (run3)**



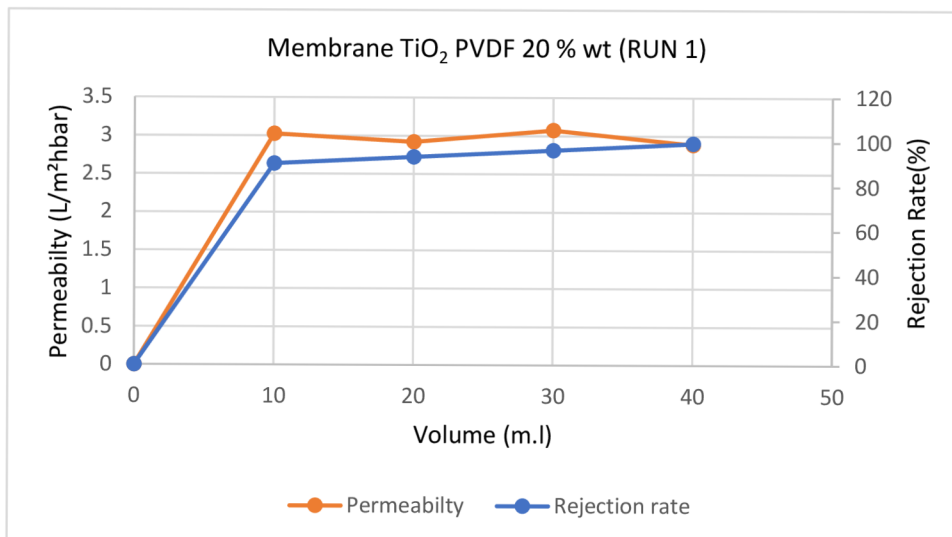
**Figure 38 Permeability and rejection of PVDF 20% wt AgNO<sub>3</sub> (run1)**



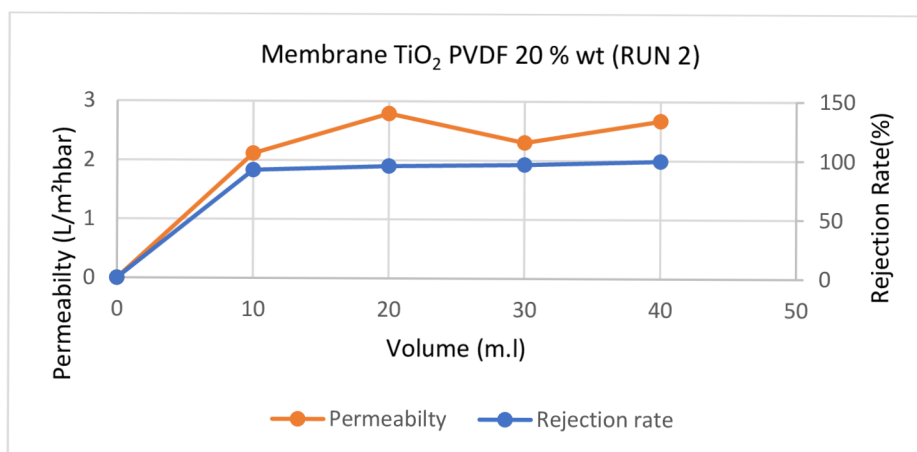
**Figure 39 Permeability and rejection of PVDF 20% wt AgNO<sub>3</sub> (run2)**



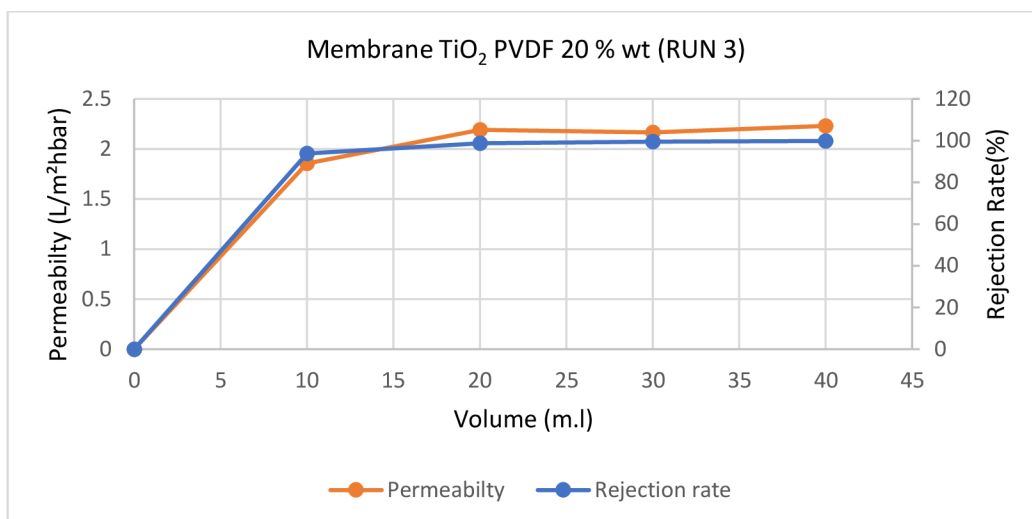
**Figure 40 Permeability and rejection of PVDF 20% wt AgNO<sub>3</sub> (run3)**



**Figure 41 Permeability and rejection of PVDF 20% wt TiO<sub>2</sub> (run1)**



**Figure 42 Permeability and rejection of PVDF 20% wt TiO<sub>2</sub> (run2)**



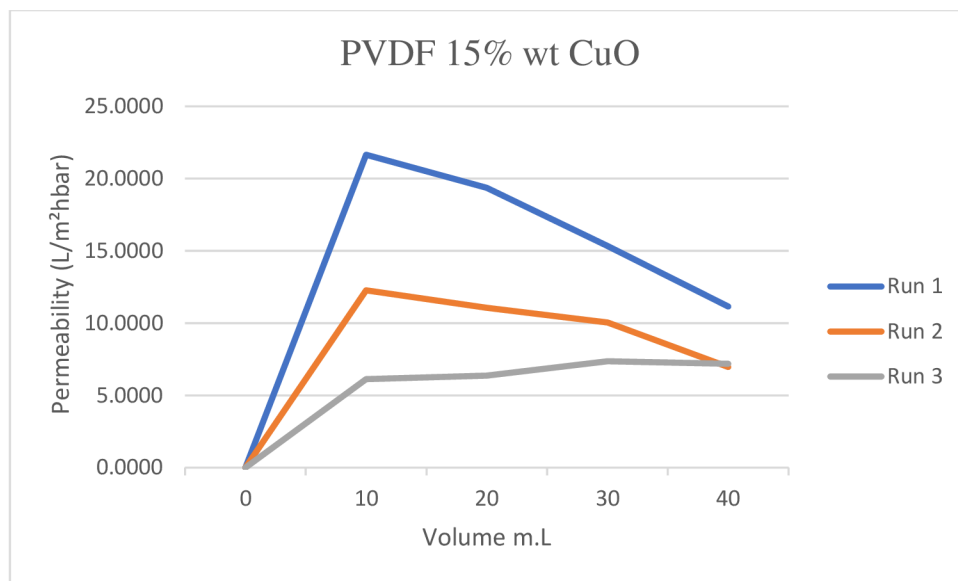
**Figure 43 Permeability and rejection of PVDF 20% wt TiO<sub>2</sub> (run3)**

These results indicate that the surface modification of PVDF leads to an increment in its antifouling properties, even when the modified membranes underwent three times the microplastic rejection runs than the unmodified ones.

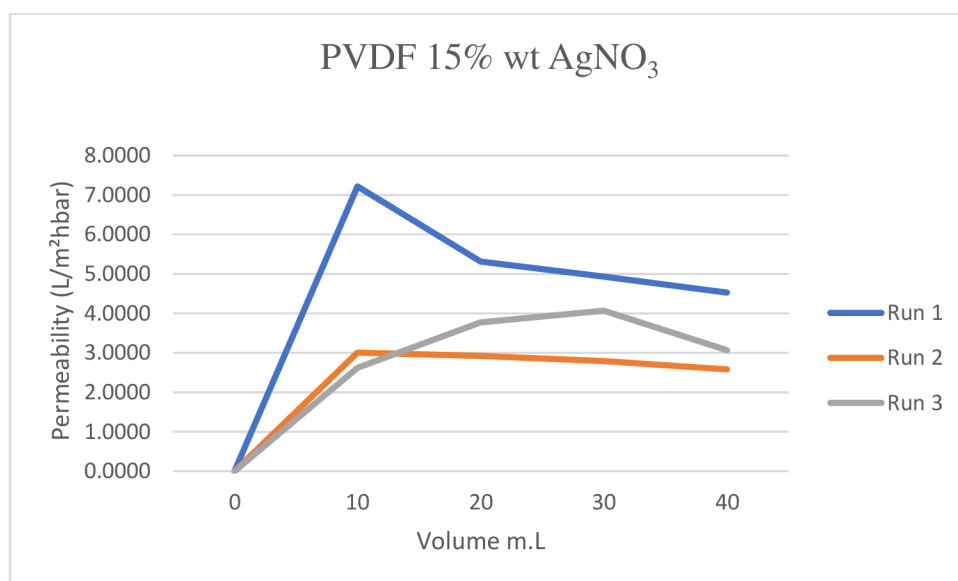
The superior permeability and microplastic rejection performance of the surface-modified PVDF 15% wt TiO<sub>2</sub> and PVDF20% wt TiO<sub>2</sub> membrane can primarily be attributed to several factors. Its larger pore size facilitates enhanced liquid flow, increasing water permeability. Additionally, the hydrophilic behavior induced by TiO<sub>2</sub> nanoparticles reduces the adhesion of microplastic particles on the membrane surface. The modified membrane exhibited reduced pore blockage, thereby maintaining water permeability over multiple usage cycles and getting a 100% rejection rate.

## 5.7 Antifouling performance of membrane

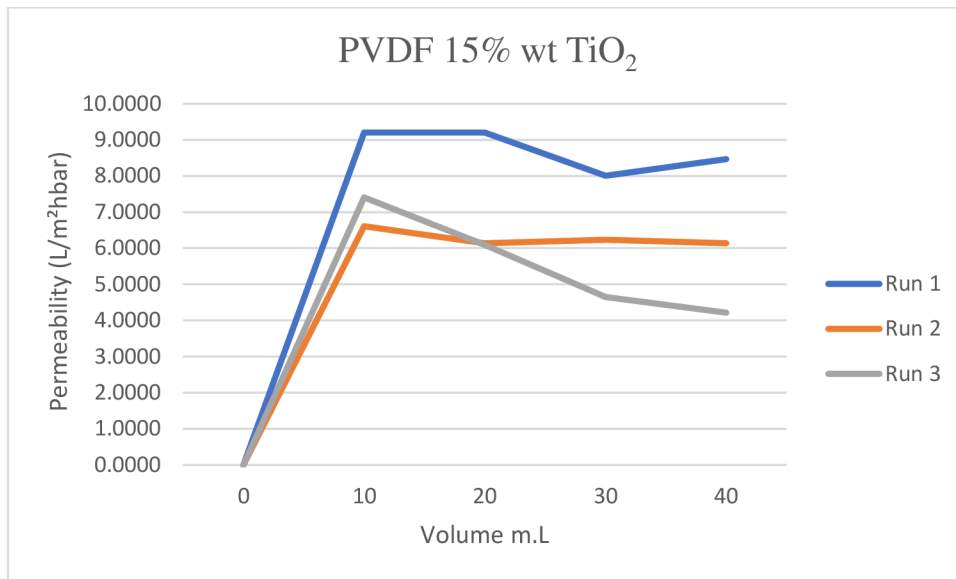
The results obtained from the microplastic rejection experiment demonstrate that both the membranes with pristine PVDF 15% wt and PVDF 20% wt experienced immediate fouling after the initial run, as illustrated in **Figure 24** for pristine PVDF 15% wt and **Figure 34** for pristine PVDF 20% wt. This phenomenon arose due to the occlusion of pores by microplastic particles, rendering both pristine PVDF 15% wt and PVDF 20% wt ineffective for the second run. Conversely, the surface-modified membrane demonstrated enhanced resistance to fouling, exhibiting a gradual fouling progression following each successive run.



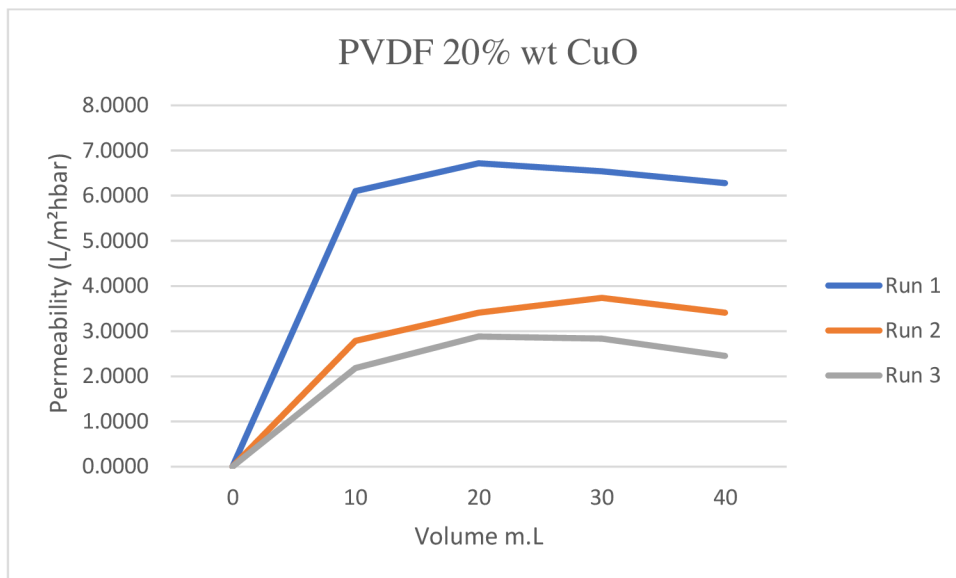
**Figure 44** Permeability, antifouling of PVDF 15% wt. CuO



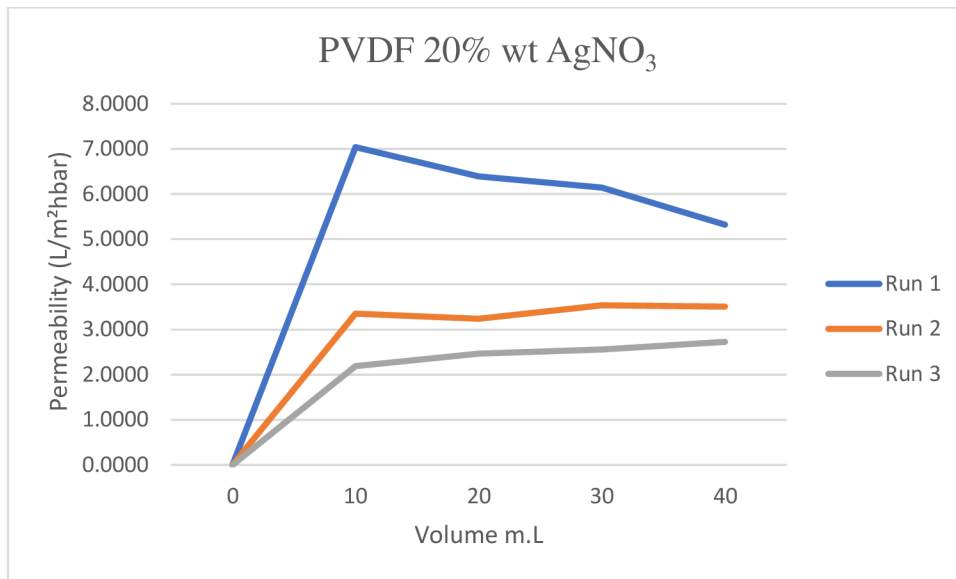
**Figure 45** Permeability, antifouling of PVDF 15% wt. AgNO<sub>3</sub>



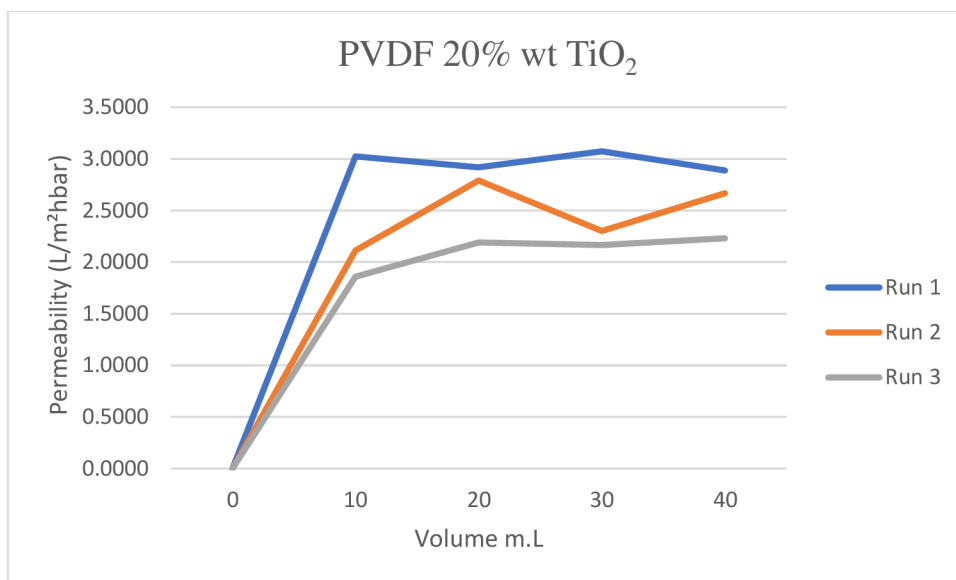
**Figure 46 Permeability, antifouling of PVDF 15% wt. TiO<sub>2</sub>**



**Figure 47 Permeability, antifouling of PVDF 20% wt CuO**



**Figure 48** Permeability, antifouling of PVDF 20% wt AgNO<sub>3</sub>



**Figure 49** Permeability, antifouling of PVDF 20% wt TiO<sub>2</sub>

The permeability results of the surface-modified PVDF membranes with 15% wt and 20% wt concentrations are compared, revealing distinct trends in performance.

For the PVDF 15% wt surface-modified membranes, **Figure 44** demonstrates the highest permeability of 12.27 (L/m<sup>2</sup>hbar) during the first run for the CuO-modified membrane, followed by a decrease to 7.18 (L/m<sup>2</sup>hbar). Similarly, **Figure 45** shows the AgNO<sub>3</sub> modified membrane achieving a peak permeability of 7.22 (L/m<sup>2</sup>hbar) in the first run, declining to 3.07 (L/m<sup>2</sup>hbar). Additionally, **Figure 46** illustrates the TiO<sub>2</sub> modified membrane reaching a maximum permeability of 9.20 (L/m<sup>2</sup>hbar) initially, then decreasing to 4.21 (L/m<sup>2</sup>hbar).

In contrast, the PVDF 20% wt surface-modified membranes, as depicted in **Figure 47**, **Figure 48**, and **Figure 49**, showcase comparable trends. The CuO-modified membrane achieved the



highest initial permeability of 6.10 (L/m<sup>2</sup>hbar), followed by a decline to 2.4 (L/m<sup>2</sup>hbar). Similarly, the AgNO<sub>3</sub> modified membrane initially exhibited a peak permeability of 7.04 (L/m<sup>2</sup>hbar), decreasing to 2.73 (L/m<sup>2</sup>hbar). Lastly, the TiO<sub>2</sub> modified membrane demonstrated an initial peak permeability of 3.02 (L/m<sup>2</sup>hbar), decreasing to 2.23 (L/m<sup>2</sup>hbar).

Overall, both PVDF 15% wt and 20% wt surface-modified membranes show similar patterns of decreasing permeability across successive runs. However, the initial permeability values differ, with the PVDF 15% wt membranes generally exhibiting higher initial permeability than the PVDF 20% wt membranes. This difference may be attributed to variations in membrane pore size, density, and surface morphology resulting from different PVDF concentrations and surface modifications.

Subsequently, the membrane becomes fouled over time. However, the results of the second and third cycles of membrane permeability indicate a similar trend.

However, the permeability decreased in the 2nd and 3rd runs, caused by membrane fouling over time. This suggests that after the cake layer on the membrane surface reaches its steady-state thickness, the membrane maintains its stable permeability. The permeability of PVDF increased by 15% after dehydrochlorination treatment and surface modification with nanoparticles and microparticles [17,33].

## 6. Conclusion and Recommendation

This thesis aimed to fabricate PVDF high-performance antifouling membrane preparation for microplastic removal. Micro and nano-particles enhanced the membrane's antifouling properties, changed membranes' surface properties and hydrophilicity with PVDF 15% wt and PVDF 20% wt.

The performance of both PVDF 15% and PVDF 20% wt modified membrane were analyzed and characterized with SEM-EDS, pore size, FTIR, water contact angle, and swelling test. SEM\_EDS test confirmed the micro and nanoparticle presence on the membrane surface, again confirmed by the SEM image. A significant change on the membrane surface was seen by SEM image. Alkaline treatment induces a process whereby the fluorine groups inherent in PVDF undergo defluorination. This defluorination involves the exchange of fluorine (F) with hydroxyl (-OH) functional groups, thereby introducing hydrophilic properties to the PVDF surface. FTIR analysis confirms the -OH group in the membrane surface after surface modification. Water contact angle measurements indicate a rise in membrane hydrophilicity after modification. The water contact angle measurements indicate a rise in membrane hydrophilicity after modification. The membranes remained stable even after being submerged in water, with no significant alterations detected in these characteristics. This implies that the membrane preserves its structural integrity and stability when exposed to aqueous environments, highlighting its appropriateness for water treatment.

These membrane characterization results showed that modified membranes exhibit improved antifouling properties and maintain stable rejection rates even after using three runs.

Subsequently, as expected, the PVDF 15% wt and PVDF 20% wt modified membranes gave 100% and 99% rejection rates, respectively. These findings highlight the potential of TiO<sub>2</sub> modification for effective microplastic rejection in water treatment processes.

PVDF membranes at a 15% weight concentration initially had higher permeability than those at a 20% concentration, regardless of surface modifications. However, the membrane fouled over time, and despite this, its permeability remained stable. This indicates that once the cake layer on the membrane surface attains a steady-state thickness, the membrane sustains its consistent permeability.

Despite exhibiting lower permeability, the membranes demonstrated impressive rejection rates, particularly those modified with TiO<sub>2</sub> nanoparticles. This suggests that the surface modifications effectively enhanced the membranes' ability to reject microplastics, compensating for their initial lower permeability.

For comparison, the PVDF 15% wt and PVDF 20% wt modified membranes had similar rejection rates, showing the potential advantage of using micro and nanoparticles for membrane modification.

This experiment made a significant impact in the field of microplastic rejection from water. It offers a promising solution to microplastic pollution in water by developing PVDF membranes with enhanced antifouling properties. This experiment was done at a laboratory scale, but after seeing the rejection rate and stable permeability performance of the membrane, it could be suggested. Changing PVDF, micro, and nanoparticle concentrations can enhance selected membrane permeability and antifouling properties. Also, different nanoparticles can be tried.

These membranes have the potential to be implemented in water treatment systems, helping purify drinking water and safeguarding aquatic ecosystems from the harmful effects of microplastic contamination. In the future, better results can be achieved by changing the concentration and micro and nano-particles.

## 7. Reference

1. Torres-Mendieta, R. *et al.* (2020) 'PVDF nanofibrous membranes modified via laser-synthesized ag nanoparticles for a cleaner oily water separation,' *Applied Surface Science*, 526, p. 146575. doi:10.1016/j.apsusc.2020.146575.
2. Acarer, S. (2023) 'A review of microplastic removal from water and wastewater by Membrane Technologies', *Water Science & Technology*, 88(1), pp. 199–219. doi:10.2166/wst.2023.186.
3. Obotey Ezugbe, E. and Rathilal, S. (2020) 'Membrane Technologies in wastewater treatment: A Review', *Membranes*, 10(5), p. 89. doi:10.3390/membranes10050089
4. STRATHMANN, H.S. (1980) MEMBRANE SEPARATION PROCESSES [Preprint].
5. Patterson, B. (2021) MEMBRANE FILTRATION OF MICROPLASTIC FIBERS: ASSESSMENT OF MEMBRANE, MICROPLASTIC, AND SOLUTION PROPERTIES, pp. xii–80.
6. Strathmann, H. (2011) 'Membrane separation processes, 3. membrane preparation and membrane module constructions', *Ullmann's Encyclopedia of Industrial Chemistry* [Preprint]. doi:10.1002/14356007.o16\_o04.
7. HUGHES, P.R. (1996) Industrial Membrane Separation Technology [Preprint]. doi:10.1007/978-94-011-0627-6.
8. kroonenberg, prof. Dr. ir. H.H. van Den (1982) phase separation phenomena in cellulose acetate solution concerning asymmetric membrane formation [Preprint].
9. Reuvers, Albertus Johannes (1987) membrane formation diffusioninduse demixing processes in the ternary polymeric system [Preprint].
10. Akarsu, C., Kumbur, H. and Kideys, A.E. (2021) 'Removal of microplastics from wastewater through electrocoagulation-electroflotation and membrane filtration processes,' *Water Science and Technology*, 84(7), pp. 1648–1662. doi:10.2166/wst.2021.356.
11. Poerio, Piacentini, and Mazzei (2019) 'Membrane processes for microplastic removal,' *Molecules*, 24(22), p. 4148. doi:10.3390/molecules24224148.
12. Pirc, U. *et al.* (2016) 'Emissions of microplastic fibers from microfiber fleece during domestic washing,' *Environmental Science and Pollution Research*, 23(21), pp. 22206–22211. doi:10.1007/s11356-016-7703-0.
13. Talvitie, J. *et al.* (2017a) 'Solutions to microplastic pollution – removal of microplastics from wastewater effluent with Advanced Wastewater Treatment Technologies,' *Water Research*, 123, pp. 401–407. doi: 10.1016/j.watres.2017.07.005.
14. (No date) Hashim, N.A.B., 2011. *Fabrication of Poly (Vinylidene Fluoride) (PVDF) Membranes*.
15. Wu, T. *et al.* (2020) 'A flexible film bulk acoustic resonator based on  $\beta$ -phase polyvinylidene fluoride polymer,' *Sensors*, 20(5), p. 1346. doi:10.3390/s20051346.

16. Wu, T. *et al.* (2020) 'A flexible film bulk acoustic resonator based on  $\beta$ -phase polyvinylidene fluoride polymer,' *Sensors*, 20(5), p. 1346. doi:10.3390/s20051346.
17. Boyraz, E. *et al.* (2019) 'Surface-modified nanofibrous PVDF membranes for liquid separation technology,' *Materials*, 12(17), p. 2702. doi:10.3390/ma12172702.
18. Méricq, J.-P. *et al.* (2015) 'High-performance PVDF-TiO<sub>2</sub> membranes for water treatment,' *Chemical Engineering Science*, 123, pp. 283–291. doi:10.1016/j.ces.2014.10.047.
19. Kitchener, B.G., Wainwright, J. and Parsons, A.J. (2017) 'A review of the principles of turbidity measurement,' *Progress in Physical Geography: Earth and Environment*, 41(5), pp. 620–642. doi:10.1177/0309133317726540.
20. Bin Omar, A. and Bin MatJafri, M. (2009) 'Turbidimeter design and analysis: A review on optical fiber sensors for the measurement of water turbidity,' *Sensors*, 9(10), pp. 8311–8335. doi:10.3390/s91008311.
21. Pal, L. and Joyce, M. (2009) 'A Simple Method for Calculation of the Permeability Coefficient of Porous Media,' *Sensors*, 9(10), pp. 8311–8335. doi:10.3390/s91008311.
22. Akarsu, C., Kumbur, H. and Kideys, A.E. (2021) 'Removal of microplastics from wastewater through electrocoagulation-electroflotation and membrane filtration processes,' *Water Science and Technology*, 84(7), pp. 1648–1662. doi:10.2166/wst.2021.356.
23. Vatanpour, V. *et al.* (2022) 'Cellulose acetate in the fabrication of polymeric membranes: A Review,' *Chemosphere*, 295, p. 133914. doi:10.1016/j.chemosphere.2022.133914.
24. Dallaev, R. *et al.* (2022) 'Brief review of PVDF properties and applications potential,' *Polymers*, 14(22), p. 4793. doi:10.3390/polym14224793.
25. Samree, K. *et al.* (2020) 'Enhancing the antibacterial properties of PVDF membrane by hydrophilic surface modification using titanium dioxide and silver nanoparticles,' *Membranes*, 10(10), p. 289. doi:10.3390/membranes10100289.
26. Woo, S.H., Park, J. and Min, B.R. (2015) 'Relationship between permeate flux and surface roughness of membranes with similar water contact angle values,' *Separation and Purification Technology*, 146, pp. 187–191. doi:10.1016/j.seppur.2015.03.048.
27. Torres-Mendieta, R. *et al.* (2020a) 'PVDF nanofibrous membranes modified via laser-synthesized Ag nanoparticles for a cleaner oily water separation,' *Applied Surface Science*, 526, p. 146575. doi:10.1016/j.apsusc.2020.146575.
28. Balzamo, G. *et al.* (2018) 'Bioinspired Poly(vinylidene fluoride) membranes with the directional release of therapeutic essential oils,' *Langmuir*, 34(29), pp. 8652–8660. doi:10.1021/acs.langmuir.8b01175.

29. Woo, S.H., Min, B.R. and Lee, J.S. (2017) 'Change of surface morphology, permeate flux, surface roughness, and water contact angle for membranes with similar physicochemical characteristics (except surface roughness) during microfiltration,' *Separation and Purification Technology*, 187, pp. 274–284. doi:10.1016/j.seppur.2017.06.030.
30. Torres-Mendieta, R. *et al.* (2020) 'PVDF nanofibrous membranes modified via laser-synthesized ag nanoparticles for a cleaner oily water separation,' *Applied Surface Science*, 526, p. 146575. doi:10.1016/j.apsusc.2020.146575.
31. Marino, T., Russo, F. and Figoli, A. (2018) 'The formation of polyvinylidene fluoride membranes with tailored properties via vapor/non-solvent induced phase separation,' *Membranes*, 8(3), p. 71. doi:10.3390/membranes8030071.
32. Pramono, E. *et al.* (2017) 'Effects of PVDF concentration on the properties of PVDF membranes,' *IOP Conference Series: Earth and Environmental Science*, 75, p. 012027. doi:10.1088/1755-1315/75/1/012027.
33. Pramanik, B.K., Pramanik, S.K. and Monira, S. (2021) 'Understanding the fragmentation of microplastics into nano-plastics and removal of nano/microplastics from wastewater using membrane, air flotation, and nano-ferrofluid processes,' *Chemosphere*, 282, p. 131053. doi:10.1016/j.chemosphere.2021.131053.
34. Le, L.-T. *et al.* (2023) 'Membrane and filtration processes for microplastic removal,' *Current Developments in Biotechnology and Bioengineering*, pp. 203–220. doi:10.1016/b978-0-443-19180-0.00019-5.
35. Nawi, N.I. *et al.* (2021) 'Polyvinylidene fluoride membrane via vapor induced phase separation for oil/water emulsion filtration,' *Polymers*, 13(3), p. 427. doi:10.3390/polym13030427.
36. Saxena, P. and Shukla, P. (2021) 'A comprehensive review on fundamental properties and applications of poly(vinylidene fluoride) (PVDF),' *Advanced Composites and Hybrid Materials*, 4(1), pp. 8–26. doi:10.1007/s42114-021-00217-0.
37. Trang Nguyen, T.D. (2022) *Preparation and Characterization of Membranes Formed by Non-Solvent Induced Phase Separation Technique* [Preprint].
38. (No date) *Thermo Fisher Scientific - US*. Available at: <https://www.thermofisher.com/> (Accessed: 12 May 2024).
39. Domaradzki, J. *et al.* (2011) 'Long-term stability of gasochromic effect in TiO<sub>2</sub>:(W, Cr, Mo) thin film', *2011 International Students and Young Scientists Workshop 'Photonics and Microsystems'* [Preprint]. doi:10.1109/stysw.2011.6155835.
40. Ma, B. *et al.* (2017) 'Influence of cellulose/[bmim]cl solution on the properties of fabricated NIPS PVDF membranes,' *Journal of Materials Science*, 52(16), pp. 9946–9957. doi:10.1007/s10853-017-1150-2.

42. Li, J.-H. *et al.* (2013) 'The double effects of silver nanoparticles on the PVDF membrane: Surface hydrophilicity and antifouling performance', *Applied Surface Science*, 265, pp. 663–670. doi:10.1016/j.apsusc.2012.11.072.
43. Wang, X. *et al.* (2022) 'Photocatalytic and antifouling properties of tio<sub>2</sub>-based photocatalytic membranes', *Materials Today Chemistry*, 23, p. 100650. doi:10.1016/j.mtchem.2021.100650.
44. Nasrollahi, N. *et al.* (2019) 'Development of hydrophilic microporous Pes ultrafiltration membrane containing cuo nanoparticles with improved antifouling and Separation Performance', *Materials Chemistry and Physics*, 222, pp. 338–350. doi:10.1016/j.matchemphys.2018.10.032.
46. Songping, W. and Shuyuan, M. (2005) 'Preparation of ultrafine silver powder using ascorbic acid as reducing agent and its application in MLCI', *Materials Chemistry and Physics*, 89(2–3), pp. 423–427. doi:10.1016/j.matchemphys.2004.09.026.
47. Cui, Z. *et al.* (2015) 'Crystalline polymorphism in poly(vinylidene fluoride) membranes', *Progress in Polymer Science*, 51, pp. 94–126. doi:10.1016/j.progpolymsci.2015.07.007.
48. kumar, vikas (no date) *Nanocomposite membrane composed of nano-alumina within sulfonated PVDF-co-HFP/Nafion blend as separating barrier in single chambered microbial fuel cell* [Preprint].